Pharmata

Official journal of Atatürk University Faculty of Pharmacy

Formerly: International Journal of PharmaATA

Volume 4 • Issue 4 • October 2024

Pharmata

Editor

Yücel KADIOĞLU 🆔
Department of Analytical Chemistry, Atatürk University, Faculty of Pharmacy, Erzurum, Turkey

Section Editors

Fatma DEMİRKAYA MİLOĞLU 🆔
Department of Analytical Chemistry, Atatürk University, Faculty of Pharmacy, Erzurum, Turkey

Nurcan KILIÇ BAYGUTALP 🆔
Department of Biochemistry, Atatürk University, Faculty of Pharmacy, Erzurum, Turkey

Rüstem Anıl UĞAN 🆔
Department of Pharmacology, Atatürk University, Faculty of Pharmacy, Erzurum, Turkey

Technical Editors

Amine Sena AYDIN 🆔
Department of Department of Pharmaceutical Chemistry, Atatürk University, Faculty of Pharmacy, Erzurum, Turkey

Language Editors

Burak BAYRAK 🆔
Department of Analytical Chemistry, Atatürk University, Faculty of Pharmacy, Erzurum, Turkey

Pharmata

Pharmata

ABOUT THE PHARMATA

Pharmata is a peer reviewed, open access, online-only journal published by the Atatürk University.

Pharmata is a quarterly journal that is published in English in January, April, July, and October.

Journal History
As of 2023, the journal has changed its title to Pharmata.

Current Title
Pharmata
EISSN: 2980-1966

Previous Title (2021-2022)
International Journal of PharmATA EISSN: 2791-9196

Abstracting and Indexing
Pharmata is covered in the following abstracting and indexing databases;
- EBSCO

Aims, Scope, and Audience
Pharmata aims to contribute to the scientific literature by publishing manuscripts of the highest caliber. The journal accepts research articles, reviews, and short communications that adhere to ethical guidelines.
The scope of the journal encompasses various topics, including but not limited to:

1. Pharmaceutical analysis of complex systems
2. Quality control and methods for biotech drugs
3. Action mechanisms and metabolism of drugs in the body
4. Quantitative and qualitative analysis in the drug screening process
5. Molecular pharmacology
6. Biopharmaceutics
7. Pharmacognosy
8. Pharmaceutical botany
9. Pharmaceutical technology studies
10. Clinical laboratory and bioanalysis
11. Pharmacological studies
12. Toxicological studies
13. Analytical chemistry techniques and methods
14. New biochemistry methods for pharmaceutical analysis
15. Rapid screening methods
16. New analytical techniques and methods
17. Pharmaceutical chemistry
18. Synthesis and analysis of new drug molecules
19. Other areas: pharmaceutical solid materials (including biomaterials, polymers, and nanoparticles), biotechnology products (including genes, peptides, proteins, and vaccines), engineered cells.

The target audience of the journal includes researchers and specialists who have an interest in or are working in any of the fields covered by the journal's scope.

You can find the current version of the Instructions to Authors at https://dergipark.org.tr/tr/pub/pharmata.

Pharmata

CONTENTS

RESEARCH ARTICLES

Removal of Hazardous Methylene Blue from Aqueous Solutions by Green Citrus Mold (*Penicillium digitatum*)@Chitosan Hydrogel Beads

Şerife PARLAYICI [1] (iD)

Erol PEHLİVAN [1] (iD)

[1] Department of Chemical Engineering, Faculty of Engineering and Natural Sciences, Konya Technical University, Konya, Türkiye

ABSTRACT

Objective: This research focuses on the novel technique of using green citrus mould (GCM), namely *Penicillium digitatum*, in conjunction with chitosan (Ctsn) as a composite to extract Methylene Blue (MB) from aqueous solutions and the composite-dye interactions were assessed analytically.

Methods: FT-IR and EDX were used to analyze the chemical characteristics of the adsorbent surface. SEM was used to visualize surface morphology. Kinetic studies were carried out for the removal of MB dye from aqueous solution with the synthesized biosorbent, equilibrium isotherms were derived and adsorption mechanism was investigated. The isotherm parameters of biosorption were determined using the most widely used adsorption models.

Results: Q_{max} value of Green Citrus Mold @Chitosan Hydrogel Beads (GCM@Ctsn) from Langmuir isotherm parameters was calculated as 60.24 mg/g. The dosage of adsorbent that performed optimally was found to be 2 g/L. The pH range, between pH 6 and pH 8, was shown to be the optimal range for attaining optimum removal effectiveness. The thermodynamic data indicated that an exothermic, spontaneous reaction occurred between the MB molecules and the composite.

Conclusion: The results highlight the feasibility and usefulness of this environmentally friendly water treatment method by demonstrating its effectiveness.

Keywords: Methylene blue, Chitosan, Green citrus mold

INTRODUCTION

Over 10,000 tons of dye are used annually in the textile industry worldwide; 10-15% of this quantity ends up in effluent.[1,2] The demand for sustainable and effective wastewater treatment systems has grown due to growing concerns about contamination of the environment. Synthetic dyes are one of the most dangerous types of pollution because of their enduring nature and detrimental impact on ecosystems. Methylene Blue (MB), a dye that is frequently used in printing and textile industries, is well-known to have toxicological effects. Therefore, it is critical to find economical and environmentally beneficial ways to reduce MB contamination.

Since the discharge of many types of solid and liquid waste into waterways poses a serious risk to the environment and the health of people, contamination by wastewater is a global concern. Because of their toxicity and durability, synthetic dyes like MB when released into wastewater streams can have negative consequences. MB, a heterocyclic aromatic chemical molecule with a long history of use in scientific and commercial applications, has attracted attention due to its potential for environmental cleanup. MB is explained by its versatility, its ability to act as a dye, drug and redox indicator. Researchers are looking into sustainable methods to get rid of these types of dyes and lessen their negative effects on the environment to solve this issue. MB, a synthetic dye widely utilized in a variety of industries including textiles, printing, and water treatment, is one specific contaminant of interest. It is well recognized that MB is hazardous to aquatic life and that releasing it into waterways without the necessary treatment can harm habitats.

Ctsn, one of the most common polysaccharides in nature, is a biodegradable biopolymer molecule formed when chitin in the exoskeleton of crustaceans is deacetylated.[3,4,5] Deacetylaing chitin yields chitosan, a white, viscoelastic polysaccharide that is both biodegradable and nontoxic. Ctsn removes pollutants by creating strong chemical connections with them and acting as an adsorbent and coagulant. Negatively charged compounds, like MB, are drawn to and bonded to by its positively charged amino groups, which causes the molecules to separate from the water. This is helpful in the general decontamination of wastewater in addition to helping to remove the dye. Ctsn is an excellent choice for adsorption-based activities because of its many advantageous characteristics, which include its high surface area, abundance of amino and hydroxyl groups, and cationic nature.[6,7] Ctsn, a biopolymer, offers favorable properties such as biodegradability and biocompatibility, making it an excellent candidate for adsorption studies. There are simple, non-toxic methods to synthesize chitosan hydrogel beads.

Utilizing Green citrus mold (GCM) (*Penicillium digitatum*), a form of green mold frequently seen on citrus fruits, in conjunction with a Ctsn composite is one effective strategy that has been researched. GCM, sometimes known as green citrus mold, is this interesting microbiological agent. This fungus is well-known for its part in food spoiling, but it also has metabolic and enzymatic properties that make it useful in a variety of biotechnological applications, such as the removal and degradation of contaminants from watery environments. Because of its resilience and versatility, it is a great choice for cleaning up pollution. GCM is a common post-harvest pathogen of citrus and has several intrinsic qualities that make it a good choice for adsorption methods, such as its low cost, abundance in nature and environmental friendliness. Food deterioration is frequently caused by penicillium fungus, particularly in fruits and vegetables. Typically, citrus is attacked by Penicillium italicum and GCM. GCM is more prone to developing rots than Penicillium italicum. The fruit wounds allow the fungi to spread their infection, although contact infection is also possible. Green mold GCM and blue mold (Penicillium italicum) are two of the post-harvest diseases that cause the most financial harm to the citrus fruit trade.[8]

Conventional physicochemical techniques for removing dyes from water include electrochemical, coagulation-flocculation, and adsorption.[9] The primary drawbacks of these techniques are their high prices and rapid sludge regeneration. Consequently, the biological processes that decolorized and/or degrade these pigments might be effective strategies to reduce their negative effects.[10] Microorganisms have garnered significant interest in the cleanup of heavy metals due to their broad availability, inexpensive cost, and high sorption capability.[11]

GCM@Ctsn hydrogel beads combine to provide an innovative way to remove organic dyes from aqueous solutions, including MB. GCM can provide enhanced adsorption capacities when immobilized in Ctsn hydrogel beads due to the synergistic effects of the microbe and the biopolymer matrix. One possible strategy is to use fungal species such as GCM in combination with Ctsn. Crab shells are the source of Ctsn, a biopolymer that occurs naturally. It has garnered a lot of attention lately because of its many characteristics, which include biodegradability, non-toxicity, and a significant tendency to bond with pollutants. GCM@Ctsn combine to generate a hybrid material with enhanced pollution-removal capabilities.[12]

The aim of this study was to investigate the kinetic behavior, isotherms, and adsorption mechanism of MB elimination process by green citrus mold immobilized in Ctsn hydrogel beads. It is essential to comprehend the underlying basic processes of this adsorption system to optimize its performance and investigate its potential for practical application in wastewater treatment. The experimental setup involved the determination of various parameters such as initial MB concentration, contact time, pH, temperature, and adsorbent dosage to optimize the adsorption process. This paper describes an investigation into the effectiveness of this composite in removing MB dye from water and presents a potential environmentally friendly solution. The unique characteristics of both the green mould and chitosan significantly enhance their overall adsorption capabilities. In this composite, the remarkable binding properties of Ctsn and the high adsorption capacity of GCM are effectively coupled. Together, they work in concert to effectively remove MB from aqueous medium.
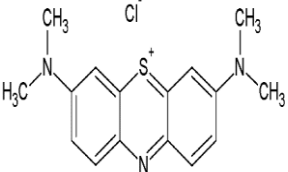
METHODS
Materials
Chitosan flakes (degree of deacetylation, DD = 75–85%) was purchased from Sigma-Aldrich Company. NaOH, HCl, and acetic acid were purchased from Merck Company. Methylene blue referred to as MB was purchased from Acros Organics (Table 1). All related chemicals used in the experiments were of analytical grade. In the preparation of the composite adsorbent, IKAMAG-RO15 model mechanical stirrer, Thermostated shaker of GFL 3033

Table 1. Main characteristics of tested MB

| Structural formula	M (g.mol^{-1})	Molecular Formula
	319.85	$C_{16}H_{18}ClN_3S \cdot xH_2O$
	Physical Form	**Solubility**
Crystalline Powder with Metal Luster		Solubility in water: soluble. Other solubilities: soluble in alcohol and chloroform, insoluble in ether
Color	**λ$_{max}$(nm)**	**Storage temp.**
Green powder	664	Room temp.

model, a pH meter (Orion 900S2) with glass electrode was used. UV-visible spectrophotometer (Schmadzu UV-1700) was used for the determination of MB (λ_{max}: 664 nm). The FT-IR spectrum was recorded by a Bruker VERTEX 70 FT-IR spectrometer. Microstructure of the Adsorbent was examined using of scanning electron microscope (SEM, Nova Nano SEM 200, FEI Company).

Synthesis of adsorbent

Green citrus mold (GCM) (*Penicillium digitatum*), a form of green mold frequently seen in citrus fruits, was obtained by keeping citrus fruits in a closed glass container for one month. It was dried at room temperature. The powder of the GCM was collected in a sealed sample tube (Figure 1). A 2% v/v acetic acid solution was used to dissolve 3 g of Ctsn, and the mixture was swirled for 24 hours to produce a transparent solution. After that, 1.5 g of dried GCM in powder form was added to the Ctsn solution and mixed for 5 hours to produce a homogenous suspension. To create composite spheres, a burette was used to drop the Ctsn@GCM mixture dropwise into a sodium hydroxide solution (600 mL methanol, 400 mL water, and 120 g of NaOH). They spent the night in a bath of NaOH. To get rid of extra acetic acid, the spheres were filtered and cleaned until the medium was neutral. The beads were stirred for 30 minutes at 60–70°C to observe the ionic crosslinking process with glutaraldehyde. The composite spheres were filtered, repeatedly cleaned in deionized water, dried at 60°C, and stored until needed after the reaction.

Experiments

The batch-shaking adsorption technique was used to conduct experiments by varying temperature, adsorbent quantity, pH, concentration, and contact duration. For pH studies, the range of 2 to 8 was selected, and for temperature, the range of 25 to 45 degrees Celsius was chosen. Using a 500 ppm stock MB solution, solutions were produced at appropriate concentrations between 25 ppm and 300 ppm. The ranges of 0.5 g/L–3.0 g/L and 5 min–240 min were used to investigate the effects of adsorbent dose and contact duration, respectively. 0.1 M
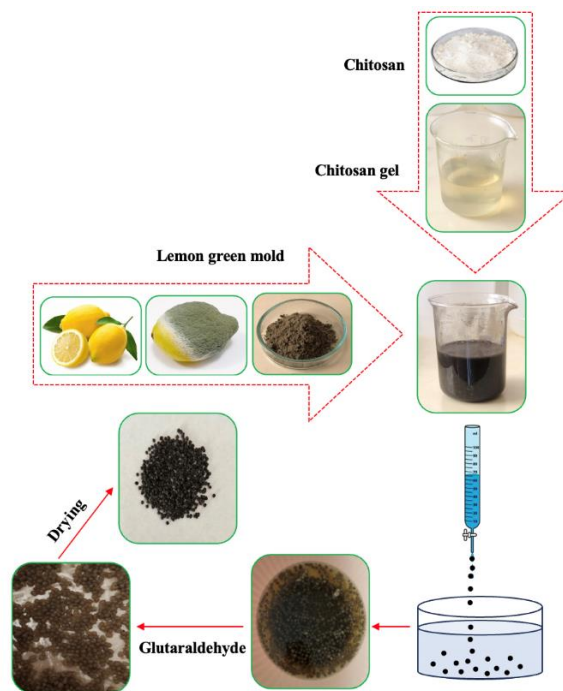
Figure 1. Schematic diagram of preparation of GCM@Ctsn beads.

HCl and 0.1 M NaOH were used to alter the pH. The samples were filtered and the residual MB concentration in the solution was computed after vigorous shaking for two hours. The concentration of dye in the solution phase was determined using a UV-Vis spectrophotometer. At 665 nm, the concentrations of MB in the solution phase were determined. Equations 1 and 2 were used to compute the equilibrium adsorption capacity (qe), which reflects the dye adsorption on the adsorbent. The chemical interactions between the dye molecules and the GCM@Ctsn beads will be investigated using Fourier-transform infrared spectroscopy (FT-IR). UV-vis spectrophotometry was used to analyze the treated solutions. The percentage of MB removed was computed using the following formula:[13]

$$q_e = (C_o - C_e)\, V/m \qquad (1)$$

$$\% \text{ Adsorption} = C_o\text{-}C_e/C_o \, x100 \qquad (2)$$

Where C_e is the equilibrium concentration of methylene blue and C_o is its starting concentration.

RESULTS

FT-IR analyses of GCM@Ctsn

The results obtained from FTIR analysis of GCM@Ctsn are shown in Figure 2. When the FT-IR spectra of GCM@Ctsn are examined, a wide absorption band in the range of 3500-3800 cm^{-1} is shown with OH and NH stretching. Various C-H stretching at 2921 cm^{-1}, C=H bond stretching (carbonyl group) at 2357 cm^{-1}, amide I vibration band[14] at 1642-1741 cm^{-1}, amide II vibration band at 1542 cm^{-1}, various C-C-H, C-O-C, C-C-O bendings and C-C, C-O stretching vibrations between 1800-1500 cm^{-1} were observed in the FT-IR spectrum.[15] The peaks at 1741, 1642, 1542, 1398, and 1238 cm^{-1} were assigned to the presence of aliphatic amines (C=O stretch), amines (N-H bend), and carboxylic acids (C-H bend, C-N stretch).[16] Furthermore, the peaks at 1044 cm^{-1} correspond to the C-O-C stretch and the peaks at 671 cm^{-1} correspond to the C-H bend planar vibrations of alkynes.
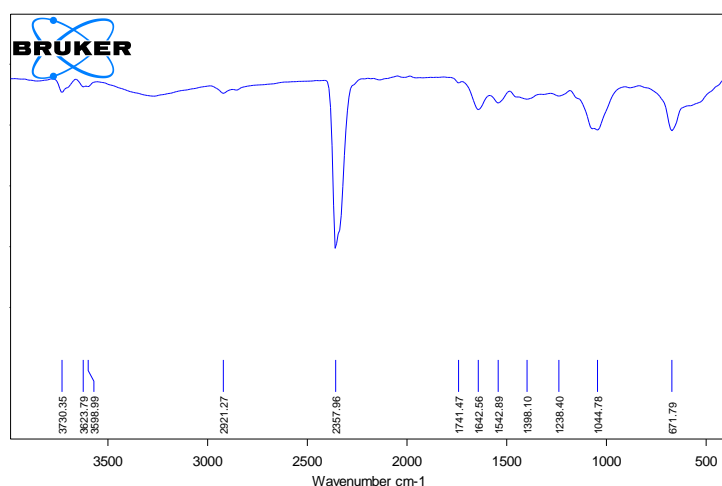
Figure 2. FTIR analysis of GCM@Ctsn

SEM analyses of GCM@Ctsn

SEM analysis was performed to obtain information about the pores formed on the surface of the adsorbent surface morphology. SEM images of GCM@Ctsn before and after MB adsorption are shown in Figure 3. When the SEM images are examined, it is seen that the GCM@Ctsn composite has a spherical structure, its surface has an irregular, hollow, indented and protruding structure and there are cavities. Figure 3a shows SEM images of the adsorbent magnified at certain ratios. These pores show that it can be used as adsorbent. These pores in the bioadsorbent structure hold the MB dye inside and on the surface. After the adsorption process, it was observed that the spherical structure remained intact in SEM images. In

addition, as can be seen in Figure 3b, MB dye was coated on the pores, making the surface smooth. It was reported that the MB dye adsorption with eucalyptus biochars resulted in a smoother surface in SEM images.[17] Similar situation was observed for the adsorption of MB dye on GCM@Ctsn surface.
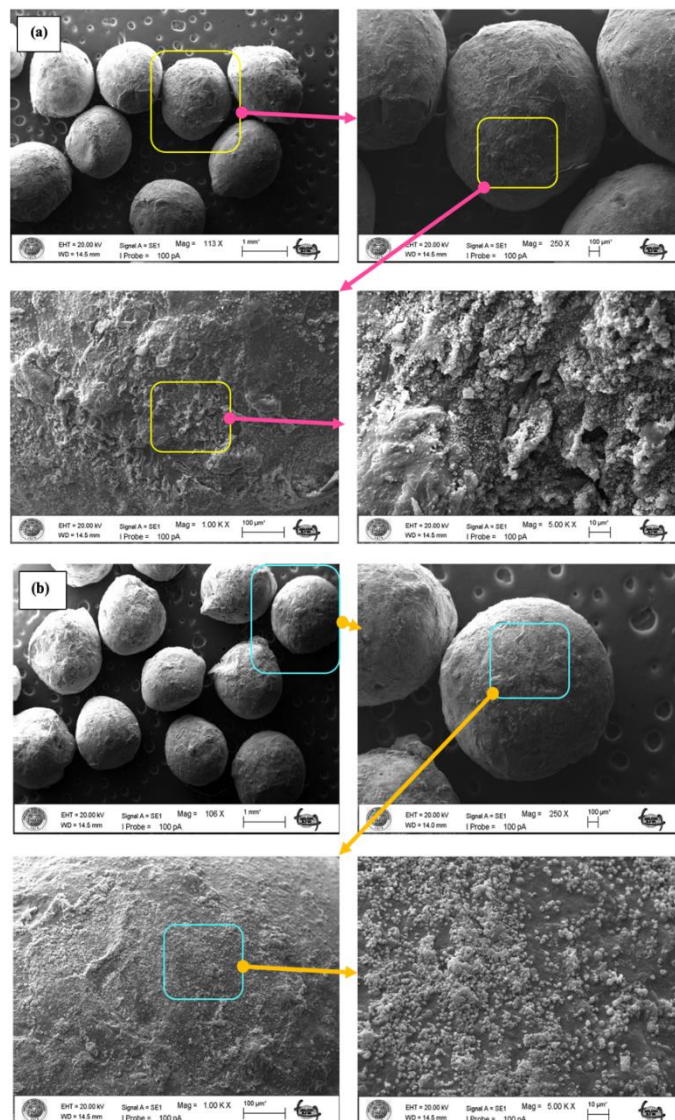
Figure 3. SEM images of GCM@Ctsn: (a) before and (b) after MB adsorption

EDX analyses of GCM@Ctsn

Energy dispersive X-ray analysis (EDX) is a method used in scanning electron microscopy to characterize the elemental composition of a sample. EDX analysis results of GCM@Ctsn before and after adsorption are given in Figure 4. It shows that 58.32% O, 33.25% C, 6.27% N and 2.16% S were present on the biosorbent surface before adsorption. These values were determined as 59.34% O, 24.99% C, 12.29% N and 3.38% S after the adsorption process (Figure 4(b)). After the analysis, the reason for the increase in the ratio of N and S in the total amount is the

N and S in the chemical structure of the adsorbed MB molecule.
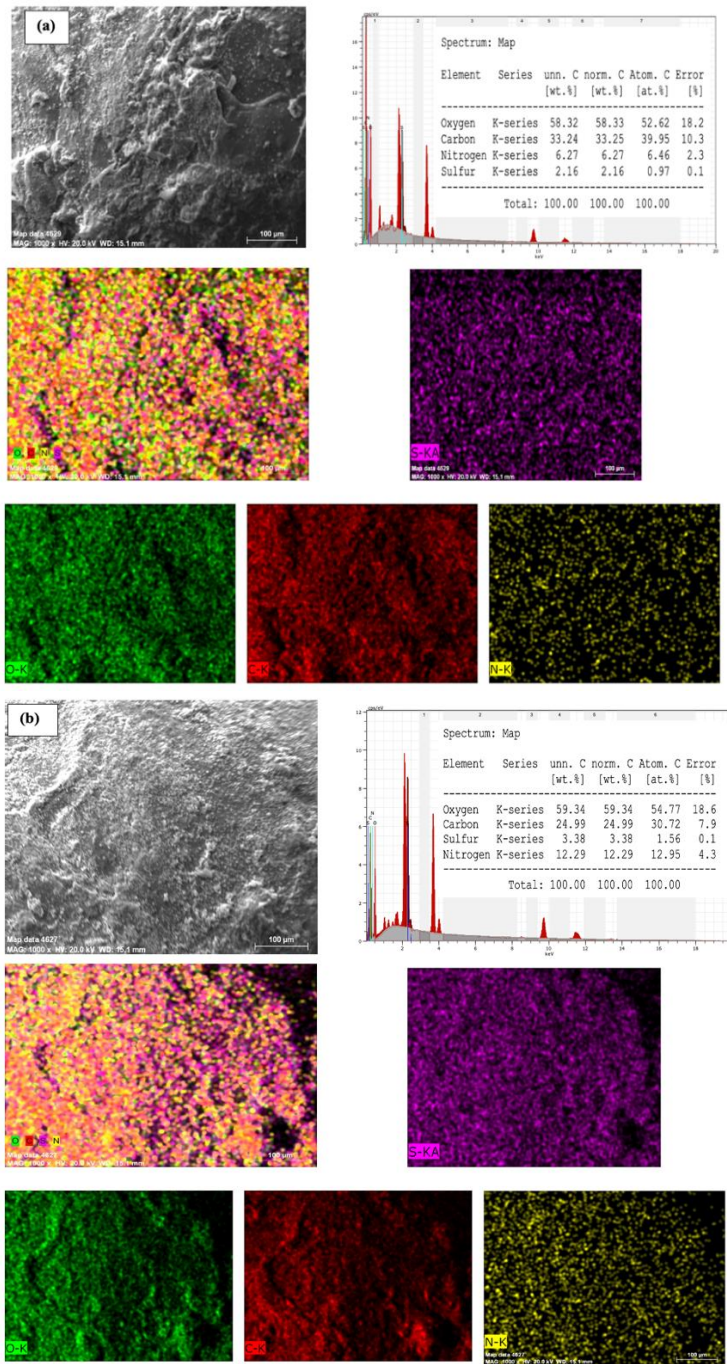
Figure 4. EDX analysis of GCM@Ctsn: (a) before and (b) after MB adsorption

Dye concentration effect and adsorption isotherms

Langmuir, Freundlich, Scatchard, D-R and Temkin isotherms are the most widely used adsorption isotherm models; each provides a distinct viewpoint on the adsorption phenomenon.[18-22] These isotherms provide important information about the mechanism and effectiveness of the adsorption process and are essential for comprehending the behavior of MB molecules when they are adsorbed onto solid surfaces like GCM@Ctsn beads.

The Langmuir isotherm model assumes that there is no interaction between the molecules of the adsorbate and monolayer adsorption onto a homogenous surface. Langmuir isotherm model, the linear formula is defined as follows (Eq. 3):

$$C_e/q_e = 1/ K_L q_m + C_e/q_m \qquad (3)$$

$$R_L = 1/ (1+K_L C_o) \qquad (4)$$

Heterogeneous surfaces and multilayer adsorption are made possible by the Freundlich isotherm. It explains the process of adsorption onto a surface with different capabilities and affinities. The Freundlich adsorption isotherm model is defined by Eq. 5.

$$\log q_e = \log K_F + 1/n \log C_e \qquad (5)$$

The Scatchard isotherm is used to explain how molecules connect to surfaces that have several binding sites. It was initially created to investigate how compounds attach to surfaces in adsorbent structures.

The Scatchard model is expressed by Eq. (6).

$$q_e/C_e = Q_s K_s - q_e K_s \qquad (6)$$

For modelling adsorption onto porous materials, another common model is the Dubinin-Radushkevich (D-R) isotherm. The D-R isotherm supports multilayer adsorption and accounts for the heterogeneity of the adsorbent surface.

The D-R isotherm model is expressed by Eq. (7)

$$\ln q_e = \ln q_m - \beta \varepsilon^2 \qquad (7)$$

The Temkin isotherm accounts for the effects of interactions between the adsorbent and the adsorbate and assumes a linear decrease in adsorption energy with surface coverage. It provides insights into the energetics of the adsorption process and the interactions between the adsorbate and the adsorbent, although it might not be suitable for systems with strong chemical interactions. The Temkin isotherm model is defined by Eq. 8.

$$q_e = B \ln K_t + B \ln C_e \qquad (8)$$

Measuring the difference in dye concentration in solution before and after treatment with the GCM@Ctsn beads allowed the removal efficiency of MB to be calculated. This was accomplished by measuring the amount of light absorbed by the dye using a UV-vis spectrophotometer.

Adsorption isotherms offer important insights into the connection between the MB concentration and the composite adsorption capability. Knowing these isotherms assists in eliminating MB by optimizing the process parameters. Plotting the quantity of MB adsorbed versus the equilibrium concentration allowed for the construction of the adsorption isotherms. Since the adsorption isotherms often displayed a characteristic shape corresponding with a Langmuir or Freundlich isotherm model, it was able to quantify the adsorption behavior and establish the maximum adsorption capacity. The adsorption behavior was analyzed using the Langmuir isotherm model.

The slope and intercept of the Langmuir isotherm equation were used to calculate the maximum adsorption capacity, also referred to as the Langmuir adsorption capacity (q_m). In this investigation, the q_m value which indicates the adsorption effectiveness of the composite material was found to be rather high, indicating that MB was effectively removed. The maximum adsorption capacity, commonly known as the Langmuir adsorption capacity (q_m), was determined using the slope and intercept of the Langmuir isotherm equation. A comparatively high qm value was found suggesting the effective elimination of MB and the adsorption efficacy of the composite material. Furthermore, the kind of adsorption was ascertained by the use of a crucial parameter that was obtained from the Langmuir isotherm model: the separation factor, also referred to as the dimensionless equilibrium parameter (R_L). The calculated R_L values in this investigation were within the range of 0 to 1, which indicates good adsorption and suggests that the method of adsorption was successful.[23] Removal efficiency is expected to rise, at least initially, with increasing MB concentrations because there are more dye molecules available for adsorption. However, further concentration improvement may not yield significant increases in efficiency once the adsorption sites on the composite surface are saturated.

Our results indicate that the removal efficiency of MB increased with increasing concentrations of MB. This suggests that higher initial concentrations of MB result in higher removal efficiency. It is important to note that the removal efficiency exhibited a diminishing rate of increase with higher MB concentrations. This could be due to the saturation of active sites available for adsorption on the GCM@Ctsn beads. As the concentration of MB surpasses the adsorption capacity, the removal efficiency tends to level off.

The concentrations of MB were measured at 25, 50, 100, 150, 200, 250, and 300 parts per million (ppm). It was blended for 120 minutes at 150 rpm, 25 °C, and a dosage of 2 g/L GCM@Ctsn beads using a shaker. The amount of dye that remained unadsorbed was calculated by measuring the absorbance of the UV-Vis. Spectrophometer. Figure 5. shows the results of a study on the effects of concentration variations on adsorption.
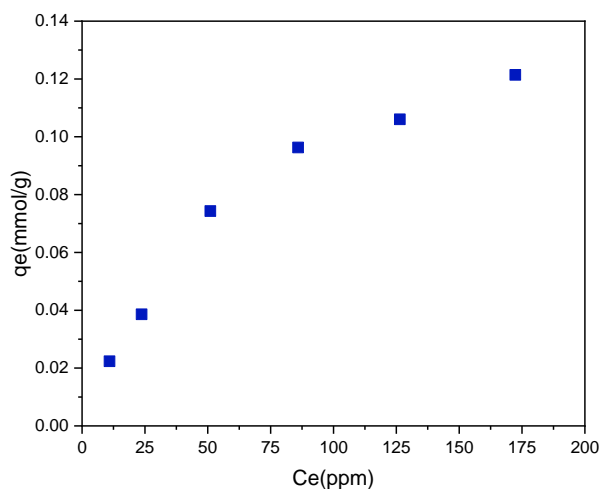
Figure 5. Influence of initial MB concentration

The determination of the interaction between adsorbate molecules and adsorbent surfaces largely depends on adsorption isotherms. Depending on the particulars of the system and the information being sought, an adsorption isotherm can be chosen to analyze the removal of dye from aqueous solutions employing adsorbents. Investigation of adsorption isotherms in the context of MB removal from aqueous solutions using GCM@Ctsn beads acting as adsorbents provides important information about the process efficiency and mechanism of adsorption. When the correlation coefficients of the isotherms were examined according to the data obtained in this study, it was seen that MB removal using GCM@Ctsn beads was more compatible with the Langmuir adsorption isotherm (Figure 6). Qmax value of GCM@Ctsn from Langmuir isotherm parameters was calculated as 60.24 mg/g (Table 2). Accordingly, we can say that adsorption for MB dyestuff occurs in specific homogeneous regions on GCM@Ctsn, and also that MB molecules are covered as a monolayer on the surface of GCM@Ctsn.

Langmuir isotherm

Freundlich isotherm

D-R

Scatchard isotherm
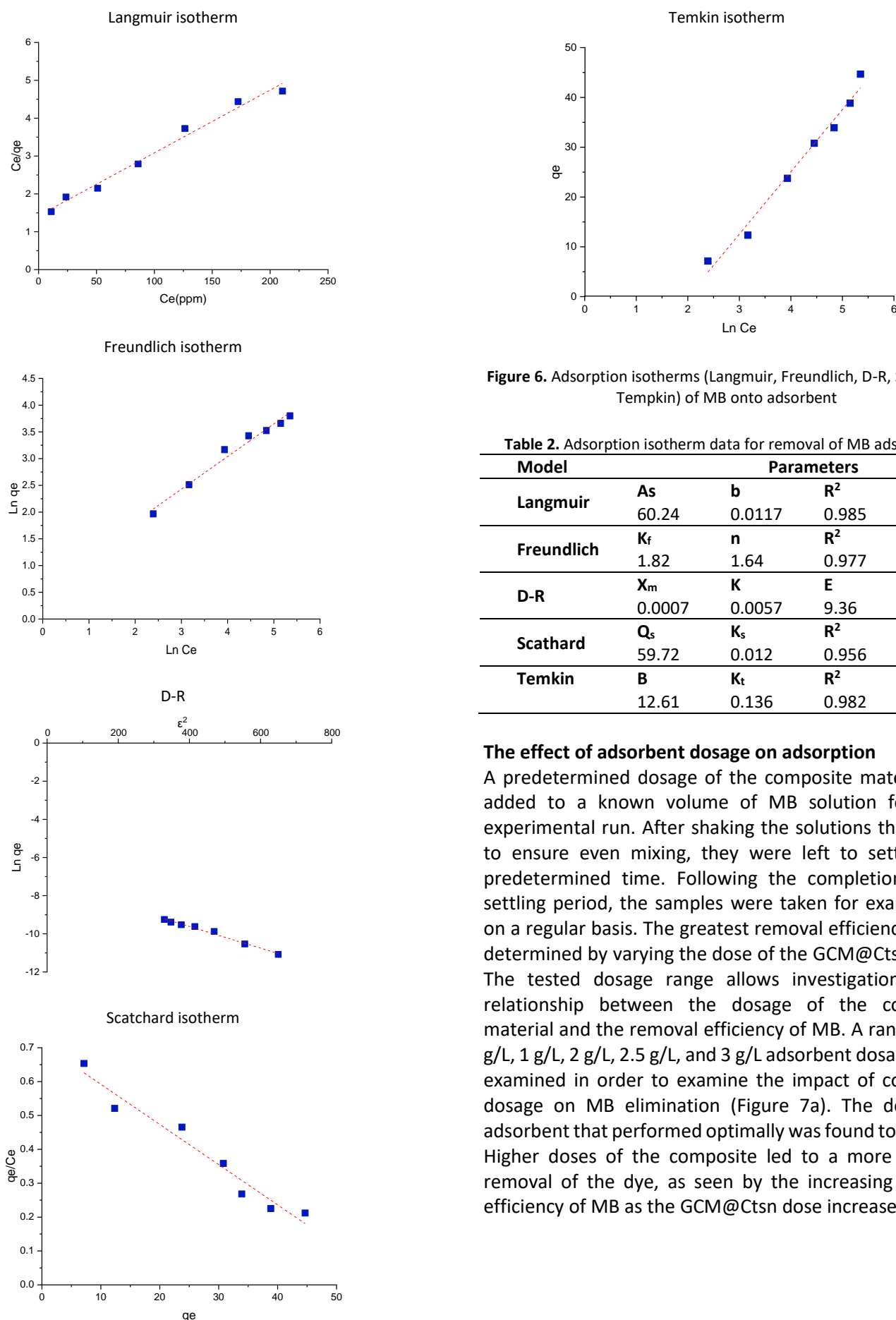
Temkin isotherm

Figure 6. Adsorption isotherms (Langmuir, Freundlich, D-R, Scatchard, Tempkin) of MB onto adsorbent

Table 2. Adsorption isotherm data for removal of MB adsorption

Model	Parameters			
Langmuir	As	b	R^2	R_L
	60.24	0.0117	0.985	0.632
Freundlich	K_f	n	R^2	
	1.82	1.64	0.977	
D-R	X_m	K	E	R^2
	0.0007	0.0057	9.36	0.987
Scathard	Q_s	K_s	R^2	
	59.72	0.012	0.956	
Temkin	B	K_t	R^2	
	12.61	0.136	0.982	

The effect of adsorbent dosage on adsorption

A predetermined dosage of the composite material was added to a known volume of MB solution for every experimental run. After shaking the solutions thoroughly to ensure even mixing, they were left to settle for a predetermined time. Following the completion of the settling period, the samples were taken for examination on a regular basis. The greatest removal efficiency can be determined by varying the dose of the GCM@Ctsn beads. The tested dosage range allows investigation of the relationship between the dosage of the composite material and the removal efficiency of MB. A range of 0.5 g/L, 1 g/L, 2 g/L, 2.5 g/L, and 3 g/L adsorbent dosages were examined in order to examine the impact of composite dosage on MB elimination (Figure 7a). The dosage of adsorbent that performed optimally was found to be 2 g/L. Higher doses of the composite led to a more efficient removal of the dye, as seen by the increasing removal efficiency of MB as the GCM@Ctsn dose increased.
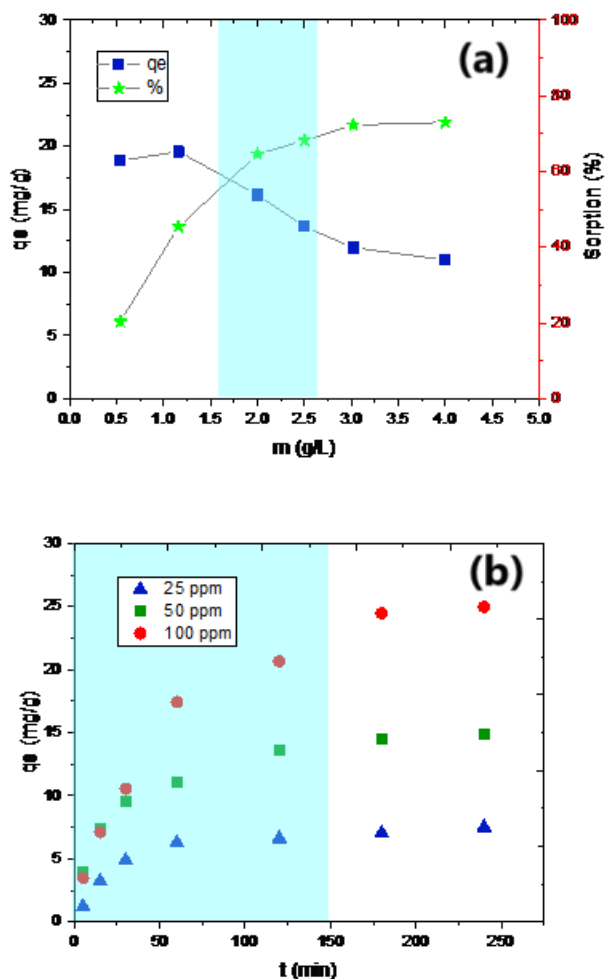
Figure 7. Adsorption of MB on the surface of GCM@Ctsn beads: (a) effect of adsorbent dosage, (b) effect of contact time

The effect of contact time on adsorption
Temperature, pH, and the duration of the contact were found to have a significant impact on the adsorption of MB onto the GCM@Ctsn.[24] Knowing the relationship between contact time and dye adsorption is necessary to optimize both the design and performance of dye removal processes. It was found that as the duration of contact was examined, the adsorption capacity rose over time until reaching equilibrium. The length of time interactions is allowed to occur directly affects how effective the adsorption process is. Due to the large number of active sites available for adsorption on the surface of the GCM@Ctsn, the dye adsorption rate is usually high at first. However, as time passes, fewer vacant active sites remain, reducing the dye adsorption rate. This implies that the GCM@Ctsn needs enough time to draw out the dye from the solution. Longer contact times may increase adsorption capacity and improve removal efficiency, according to the data.

The efficiency of the adsorption process is directly impacted by the amount of time interactions are permitted to take place. The dye adsorption rate is often high at initially because the surface of the composite has a large number of active sites that are available for adsorption. But as time goes on, the number of unoccupied active sites decreases, which lowers the dye adsorption rate. The elimination percentage of MB improved steadily during the course of the contact duration. This suggests that the GCM@Ctsn was successfully saturating the dye molecules by adsorption. Higher clearance percentages were achieved because the extended contact time for more thorough adsorption.

At various contact durations (5, 15, 30, 60, 120, 180, and 240 min.), 2 g/L GCM@Ctsn dose, natural pH of the solution, 25 °C, and 150 ppm, the impact of contact time on MB adsorption was investigated (Figure 7b). Examining the Figure 7. reveals that in the first thirty minutes, the MB dye adsorption on the composite adsorbent sample grows quickly, and in the next 120 minutes, it nearly achieves equilibrium. The adsorption time was found to be 120 minutes for the time it took to achieve equilibrium.

Effect of pH on adsorption
The pH of the solution is significant and a key factor in the dye removal processes because it influences the surface charge of the adsorbent and the dye molecule.[25] Comprehending this impact is crucial for customizing the adsorption procedure to attain optimal elimination efficacy. The solubility of the adsorbent and the surface charge of the contaminant are directly influenced by pH. Near-neutral pH values yielded the best acceptance effectiveness. The results show that the GCM@Ctsn works best in neutral environments, which means it can be used in situations where controlling pH is difficult. The surface charge of adsorbent varies as the pH of the solution rises. GCM@Ctsn beads contain positively charged surfaces at low pH levels. The dissociation of ionizable groups in the adsorbents causes the surface charge to get more negative as the pH rises. The electrostatic interactions between the molecules of the MB dye and the adsorbent are impacted by this charge reversal process. Consequently, the pH of the solution affects the adsorption capacity.

Because different functional groups on the surface of an adsorbent are ionized and protonated as the pH of a solution changes, this has an impact on the adsorbent's surface charge. The surfaces of the GCM@Ctsn beads, which are utilized as the adsorbent, have functional groups like carboxyl, amino, and hydroxyl groups. Depending on the pH of the solution, these groups may

ionize or protonate, altering the surface charge. The solubility of MB in water is influenced by pH. The cationic form of MB predominates at lower pH levels, whereas the anionic form is prevalent at higher pH values. The ionic state change of the dye has an impact on how well it will bind to the adsorbent. By adjusting pH, the ionic state and surface charge of MB may be changed, which maximizes the adsorption capacity. The deprotonation of functional groups causes the adsorbent's surface charge to become extremely negative under high pH levels, or alkaline circumstances. The MB molecules may be repelled by this negatively charged surface, greatly reducing their adsorption ability. The adsorption process may change from electrostatic attraction to other mechanisms, such hydrophobic or π-π interactions, in alkaline circumstances. Lower removal efficiency for MB from the solution may arise from these other processes, which might not be as effective as electrostatic attraction. Changes in pH eventually impact the solubility of MB, the availability of binding sites, and the electrostatic attraction between the adsorbent and MB, which determines the efficacy of the adsorption process.

There are several reasons for the improved adsorption kinetics attained with this composite material. First off, GCM@Ctsn work together to produce a structure that is more porous and has a larger surface area. Because of its porous nature, which offers plenty of locations for adsorption, the adsorbent can interact with more dye molecules. Second, a variety of mechanisms, including electrostatic attractions, hydrogen bonds, and π-π interactions, are used by the functional groups in chitosan, such as amine and hydroxyl groups, to interact with the methylene blue dye. The enhanced adsorption capacity and kinetics of the composite material are a result of these interactions.

Using the GCM@Ctsn combination, a number of studies were carried out to ascertain the ideal pH range for the elimination of MB. Testing was done at several pH levels, from acidic to alkaline, and the effectiveness of MB removal was evaluated at each one. The experimental outcomes gathered at pH 2, 3, 4, 5, 6, 7, and 8 to observe the effect of pH on the adsorption of MB dye on the adsorbent are presented in Figure 8. The initial pH values of the solutions were found to be 6.0 for MB. It is necessary to do in-depth research on the effects of solution pH changes on MB adsorption. The pH range, between pH 6 and pH 8, was shown to be the optimal range for attaining optimum removal effectiveness. MB adsorption generally decreases noticeably at low pH levels in the solution. This process happens because the

adsorbent's surface becomes more positively charged in an acidic environment, which causes the cationic dye molecules to repel one another electrostatically. Consequently, the overall adsorption capacity diminishes as the MB's affinity for the GCM@Ctsn surface declines. This result emphasizes how crucial pH regulation is to maximizing the effectiveness of dye removal procedures.
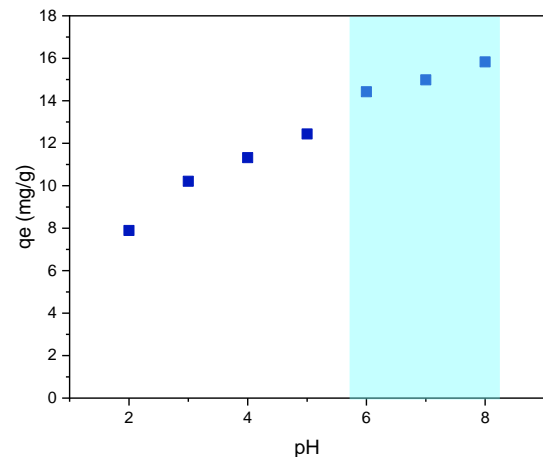
Figure 8. Effect of pH on the adsorption of MB on the surface of GCM@Ctsn beads

Adsorption kinetics

The study of how quickly and effectively a substance adsorbs or sticks to the surface of a solid material is known as adsorption kinetics (Figure 9). A common dye used in many different businesses is MB, which has been linked to possible environmental impacts. One popular kinetic model for explaining the adsorption process onto solid surfaces is the Elovich model. It is appropriate for a range of adsorption systems since it integrates both chemical and physical adsorption pathways (Table 3).
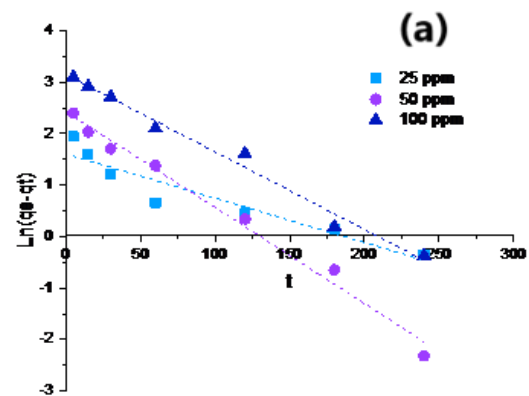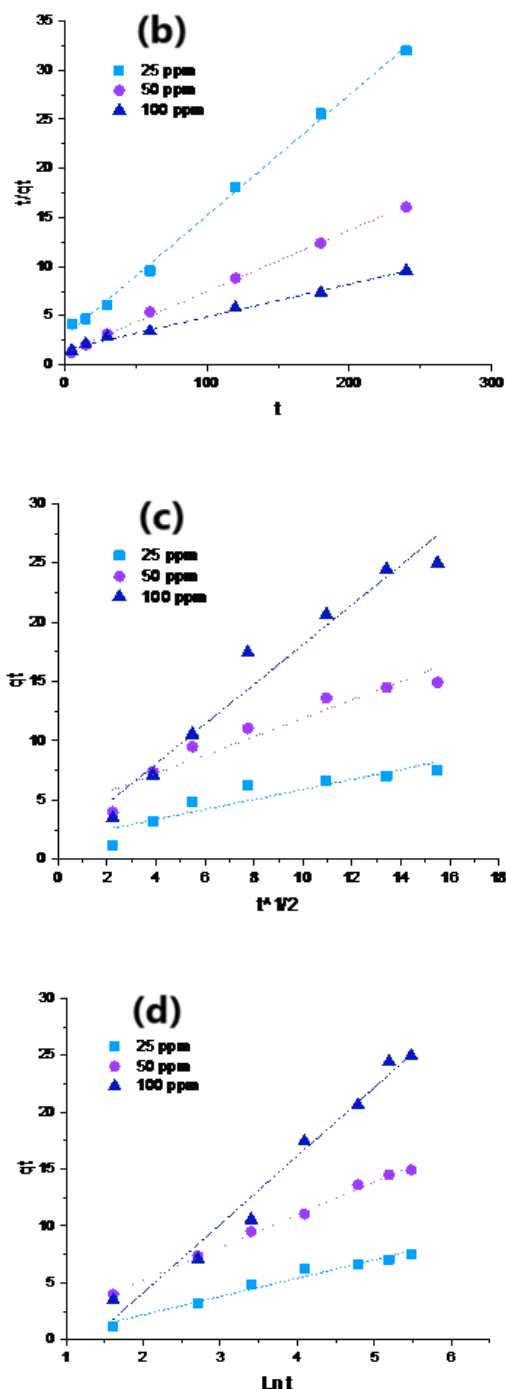
Figure 9. Kinetic models (pseudo-first-order kinetic model (a) pseudo-second-order kinetic model (b) intra-particle diffusion model (c) and elovich model (d)) for MB adsorption onto GCM@Ctsn beads

$$In\,(q_e - q_t) = Inq_e - k_1 t \qquad (9)$$

$$\frac{1}{q_t} = \frac{1}{k_2\;qe^2} + \frac{1}{q_e\,t} \qquad (10)$$

Elovich model was expressed using the following (Eq.11):

$$q_t = \frac{ln\alpha\beta}{\beta} + \frac{lnt}{\beta} \qquad (11)$$

Weber and Morris formulate the intra-particle diffusion model to locate the migration of adsorbates from the surface of adsorbent into its internal pores because of stirring process as follows (Eq. 12):

$$q_t = k_{id}t^{0.5} + C \qquad (12)$$

Table 3. Kinetic model parameter for MB removal

Kinetics modeling	Parameters	C_o(ppm)	
	$q_{e\ exp}$	25	8.2
		50	15.1
		100	25.7
	k_1	25	0.0086
		50	0.0187
Pseudo First-order		100	0.015
	q_e	25	4.99
		50	11.39
		100	23.38
	R^2	25	0.900
		50	0.987
		100	0.985
	k_2	25	0.0052
		50	0.0031
		100	0.0007
	q_e	25	8.13
Pseudo Second- order		50	16.05
		100	29.94
	R^2	25	0.998
		50	0.998
		100	0.995
	α	25	1.62
		50	2.42
		100	0.85
	β	25	0.17
Elovich		50	0.35
		100	0.62
	R^2	25	0.976
		50	0.996
		100	0.969
	k_{id}	25	1.68
		50	0.78
		100	0.42
Intraparticle diffusion	C	25	1.34
		50	4.12
		100	1.68
	R^2	25	0.956
		50	0.917
		100	0.836

Thermodynamics of adsorption

Thermodynamics offers insightful information on the viability and energy of the method of adsorption. Understanding the thermodynamics of adsorption is essential to optimizing the efficiency and design of adsorption. Elevated temperatures resulted in an increased removal efficiency, subsequently impacting the adsorption capacity of the composite material. The calculation and evaluation of many thermodynamic parameters, including enthalpy (ΔH^o), entropy (ΔS^o), and Gibbs free energy (ΔG^o), are part of the investigation of thermodynamics in adsorption. The spontaneity and directionality of the adsorption process may be assessed using these parameters.

An endothermic reaction, in which the adsorbate is preferred at higher temperatures, is indicated by a positive ΔH^o. Regarding the adsorption of MB by the composite, a positive ΔS^o value indicates increased disorder during the adsorption procedure. This suggests that the adsorption of MB onto the composite surface results in a more random distribution of molecules, which increases the overall thermodynamic viability of the process. Conversely, a negative ΔH^o denotes a more advantageous exothermic reaction at lower temperatures. The type of bonding or forces at play during the adsorption process may be ascertained with the support of the enthalpy change. Gibbs free energy (ΔG^o) is a fundamental thermodynamic principle that is crucial to adsorption. The energy is available to act as a chemical reaction or physical process is represented as Gibbs-free energy. The adsorption process may be classified as spontaneous ($\Delta G^o < 0$) or non-spontaneous ($\Delta G^o > 0$) based on the change in Gibbs free energy (ΔG^o).

The impact of temperature on MB adsorption on the adsorbent surface was investigated at 25°, 35°, and 45°C. The results of the experiment are given in Table 4. The graphic illustrates how the amount of MB adsorbed on the adsorbent surface drops as temperature rises.

$$\Delta G^\circ = - RT \ln K_c \qquad (13)$$

$$In\, K_C = \frac{\Delta S^o}{R} - \frac{\Delta H^o}{RT} \qquad (14)$$

Table 4. Thermodynamic parameters for adsorption of MB onto composite bead

ΔS^o	ΔH^o	ΔG^o (J mol^{-1})			
(J K^{-1}mol^{-1})	(J mol^{-1})	T=298.15K	T=308.15K	T=318.15K	R^2
-9.62	-3505.81	-637.45	-541.25	-445.04	0.986

Recycling efficiency

The regenerative nature of the GCM@Ctsn is one of its benefits. By desorbing the MB molecules, the composite may be readily renewed after it has reached its adsorption capacity. This characteristic makes reusing possible. The adsorbents' recyclability was tested over five cycles (Figure 10). The dye-loaded adsorbent was washed in ethanol to desorb dyes after each operation. Following an overnight drying process at 50°C to eliminate any remaining moisture, the regenerated samples were preserved for use in later cycles.
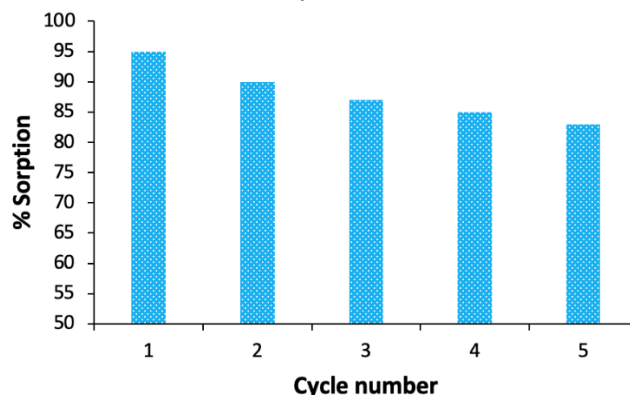
Figure 10. Desorption efficiency after recycle use

Comparison with other adsorbents

The selection of an adsorbent should take into account various criteria, not only its capacity but also its practical usage, cost of preparation, availability, and raw materials utilized in its synthesis. Numerous studies have examined the usage of various adsorbents in the removal of MB from aqueous solutions in the literature. Table 5 presents an analysis of the maximum adsorption capabilities of several adsorbents from multiple investigations conducted under optimal conditions as a consequence of these studies. The adsorption capacity of GCM@Ctsn was found to be in line with the literature when compared to the given references.

DISCUSSION

This article details an investigation on the composite's ability to remove MB dye from water as well as a potential environmentally friendly replacement. The adsorption capacity of GCM@Ctsn was greatly impacted by the medium's initial pH of 6.0. The Langmuir model was consistent with the adsorption results, which showed that a monolayer adsorption had taken place. It was demonstrated that the experimental results agreed with the PSO model. The existence of MB molecules and their uniform coating of the composite were validated by FT-IR and SEM analyses.

Table 5. Comparison of adsorption capacities of different adsorbents for MB removal

Adsorbent	q_e (mgg^{-1})	Ref.
Chitosan-nSiO$_2$ nanocomposites	31.34	[26]
nanoTiO$_2$-chitosan-plum kernel shell	86.96	[27]
Fe$_3$O$_4$/graphene/chitosan nanocomposite	94.16	[28]
Magnetic alginate-biochar from acorn cups	52.63	[25]
Chitosan magnetic composite microspheres	33.60	[29]
Lemongrass leaves	43.16	[30]
Magnetized chitosan nanocomposite	76.34	[31]
Chitosan/κ-carrageenan/acid-activated bentonite composite membranes	18.80	[32]
Fe-modified banana peel	28.1	[33]
GCM@Ctsn	60.24	*This study*

The results of this study may aid in the development of long-lasting and efficient techniques for eliminating MB and other contaminants of a similar nature from water sources. Moreover, this research can open the door to affordable and environmentally friendly remedies to water contamination by employing widely accessible and sustainable ingredients like chitosan and *Penicillium digitatum*. Removing MB from aqueous solutions by using this composite material in wastewater treatment can help reduce water pollution caused by the textile industry. It also has the potential to be used in environmental remediation, helping to purify contaminated soil and water from dye contaminants.

The adsorption capability of the composite was shown to rise with greater MB concentrations, suggesting that the composite is successful in eliminating MB from polluted water, according to the data. Furthermore, the composite material was shown to adhere to the Langmuir model, indicating monolayer adsorption behavior, as indicated by the adsorption isotherms. The amount of time required for adsorption to reach equilibrium was found to be 120 minutes. Chemisorption, electrostatic attraction and pore filling are the prominent mechanisms for MB removal. The maximum adsorption capacity was found to be 60.24 mg/g. Moreover, pH had a significant effect on adsorption efficiency, and 6.0 was the most favorable pH value. Thermodynamic properties showed that the adsorption process was endothermic and spontaneous.

REFERENCES

1. Saratale RG, Saratale GD, Chang JS, Govindwar SP. Bacterial decolorization and degradation of azo dyes: A review. *J Taiwan Inst Chem Eng*. 2011;42(1):138–157. [CrossRef]
2. Pereira L, Alves M. Dyes—environmental impact and remediation. *Environ Protec Strat Sustain Develop.* 2012;111-162. [CrossRef]
3. Satitsri S, Muanprasat C. Chitin and chitosan derivatives as biomaterial resources for biological and biomedical applications. *Molecules*. 2020;25(24):5961. [CrossRef]
4. Shahbaz U, Basharat S, Javed U, Bibi A, Yu XB. Chitosan: a multipurpose polymer in food industry. *Polym Bull.* 2023;*80*(4):3547–3569. [CrossRef]
5. Strnad S, Zemljič LF. Cellulose–chitosan functional biocomposites. *Polymers*. 2023;15(2):425. [CrossRef]
6. Perumal S, Atchudan R, Yoon DH, Joo J. Cheong W. Spherical chitosan/gelatin hydrogel particles for removal of multiple heavy metal ions from wastewater. *Ind Eng Chem Res*. 2019;58:9900–9907. [CrossRef]
7. Thambiliyagodage C, Jayanetti M, Mendis A, et al. Recent advances in chitosan based applications. a review. *Materials*. 2023;16(5):2073. [CrossRef]
8. Bhatta UK. Alternative management approaches of citrus diseases caused by Penicillium digitatum (green mold) and Penicillium italicum (blue mold). *Front Plant Sci*. 2022;12:833328. [CrossRef]
9. Collivignarelli MC, Abbà A, Miino MC, Damiani S. Treatments for color removal from wastewater: State of the art. *J Environ Manag.* 2019;236:727–745. [CrossRef]
10. Garg N, Garg A, Mukherji S. Eco-friendly decolorization and degradation of reactive yellow 145 textile dye by Pseudomonas aeruginosa and Thiosphaera pantotropha. *J Environ Manag.* 2020;263:110383. [CrossRef]
11. Shi F, Liu ZG, Li JL, et al. Alterations in microbial community during the remediation of a black-odorous stream by acclimated composite microorganisms. *J Environ Sci.* 2022;118:181–193. [CrossRef]
12. Singh J, Sharma P, Mishra V. Simultaneous removal of copper, nickel and zinc ions from aqueous phase by using mould. *Inter J Environ Sci Technol.* 2023;20(2):1937–1950. [CrossRef]
13. Lafi R, Montasser I, Hafiane A. Adsorption of congo red dye from aqueous solutions by prepared activated carbon with oxygen-containing functional groups and its regeneration. *Adsorpt Sci Technol.* 2019;37(1-2):160–181. [CrossRef]
14. Kurç MA, Güven K, Korcan E, Güven A, Malkoc S. Lead biosorption by a moderately halophile Penicillium sp. isolated from çamalti saltern in Turkey. *Anadolu University J Sci Technol C-Life Sci Biotechnol.* 2016;5(1):13-22. [CrossRef]
15. Ünlü CH, Pollet E, Avérous L. Original macromolecular architectures based on poly(ε-caprolactone) and poly(ε-thiocaprolactone) grafted onto chitosan backbone. *Inter J Mol Sci.* 2018;19 (12):3799. [CrossRef]

16. Preethi S, Abarna K, Nithyasri M, et al. Synthesis and characterization of chitosan/zinc oxide nanocomposite for antibacterial activity onto cotton fabrics and dye degradation applications. *Int J Biol Macromol.* 2020;164:2779-2787. [CrossRef]

17. Dawood S, Sen TK, Phan C. Adsorption removal of Methylene Blue (MB) dye from aqueous solution by bio-char prepared from *Eucalyptus sheathiana* bark: kinetic, equilibrium, mechanism, thermodynamic and process design. *Desal Water Treat.* 2016;57(59):28964-28980. [CrossRef]

18. Langmuir I. The constitution and fundamental properties of solids and liquids. *J Franklin Inst.* 1917;183(1):102–105.

19. Freundlich H. Uber die biosorption in lasungen. *J Phy Chem*. 1906;57:385–470.

20. Scatchard G. The attractions of proteins for small molecules and ions. *Ann N Y Acad Sci.* 1949;51(4):660–672.

21. Dubinin MM, Radushkevich LV. Equation of the characteristic curve of activated charcoal. *Proc Acad Sci USSR Phys Chem Sect*. 1947; *55*:331–333.

22. Temkin M, Pyzhev V. Recent modifications to Langmuir isotherms. *Acta Physiochim USSR*. 1940;12:217–222.

23. Parlayıcı Ş, Yar A, Pehlivan E, Avcı A. ZnO-TiO$_2$ doped polyacrylonitrile nano fiber-Mat for elimination of Cr (VI) from polluted water. *J Anal Sci Technol.* 2019;10:1-12. [CrossRef]

24. Parlayıcı Ş, Pehlivan E. Fast decolorization of cationic dyes by nano-scale zero valent iron immobilized in sycamore tree seed pod fibers: kinetics and modelling study. *Int J Phytorem*. 2019;21(11):1130–1144. [CrossRef]

25. Parlayıcı Ş, Pehlivan E. An ecologically sustainable specific method using new magnetic alginate-biochar from acorn cups (Quercus coccifera L.) for decolorization of dyes. *Polym Bull*. 2023;80(10):11167–11191. [CrossRef]

26. Bhattacharya S, Bar N, Rajbansi B, Das SK. Adsorptive elimination of methylene blue dye from aqueous solution by chitosan-n SiO2 nanocomposite: Adsorption and desorption study, scale-up design, statistical, and genetic algorithm modeling. *Environ Prog Sustain Energy*. 2024;43(2):e14282. [CrossRef]

27. Pehlivan E, Parlayıcı Ş. Fabrication of a novel biopolymer-based nanocomposite (nanoTiO2-chitosan-plum kernel shell) and adsorption of cationic dyes. *J Chem Technol Biotechnol.* 2021;96(12):3378–3387. [CrossRef]

28. Tran HTT, Hoang LT, Tran HV. Electrochemical synthesis of graphene from waste discharged battery electrodes and its applications to preparation of graphene/fe3o4/chitosan-nanosorbent for organic dyes removal. *Z Anorgan Allg Chem*. 2022;648(3):e202100313. [CrossRef]

29. Yan H, Li H, Yang H, Li A, Cheng R. Removal of various cationic dyes from aqueous solutions using a kind of fully biodegradable magnetic composite microsphere. *Chem Eng J.* 2013;223:402–411. [CrossRef]

30. Zein R, Purnomo JS, Ramadhani P, Alif MF, Safni S. Lemongrass (Cymbopogon nardus) leaves biowaste as an effective and low-cost adsorbent for methylene blue dyes removal: isotherms, kinetics, and thermodynamics studies. *Sep Sci Technol*. 2022;57(15):2341–2357. [CrossRef]

31. Mashkoor F, Nasar A, Jeong C. Magnetized chitosan nanocomposite as an effective adsorbent for the removal of methylene blue and malachite green dyes. *Biomass Conv Bioref*. 2024;14:313–325. [CrossRef]

32. Ulu A, Alpaslan M, Gultek A, Ates B. Eco-friendly chitosan/κ-carrageenan membranes reinforced with activated bentonite for adsorption of methylene blue. *Mater Chem Phys.* 2022;278:125611. [CrossRef]

33. Çatlıoğlu F, Akay S, Turunç E, et al. Preparation and application of Fe-modified banana peel in the adsorption of methylene blue: process optimization using response surface methodology. *Environ Nanotechnol Monit Manag.* 2021;16:100517. [CrossRef]

The Role of Insulin Receptor Substrate 4 (IRS4) Protein in the Radiotherapy Response of Glioblastoma Multiforme (GBM) Cells

Aysun ARSLAN [1] (iD)
Tahir ÇAKIR [2] (iD)
Gökhan GÖRGİŞEN [3,4] (iD)

[1]Van Yüzüncü Yıl University, Institute of Health Sciences, Deparment of Medical Biology, Van, Türkiye
[2]Van Yüzüncü Yıl University, Faculty of Medicine, Department of Biophysics, Van, Türkiye
[3]Van Yüzüncü Yıl University, Faculty of Medicine, Department of Medical Genetics, Van, Türkiye
[4]Van Yüzüncü Yıl University, Institute of Health Sciences, Department of Molecular Medicine, Van, Türkiye

ABSTRACT

Objective: To explain the fundamental role of Insulin Receptor Substrate 4 (IRS4) protein in the response of Glioblastoma Multiforme (GBM) cells to radiotherapy.

Methods: LN229 cells were transfected with IRS4 expression vector using lipofectamine, and the ectopic IRS4 expression was confirmed by western blot. After irradiating LN229 cells with 5, 8, and 10 Gy doses of radiotherapy, the functional effect of IRS4 on radiotherapy was determined using MTT and colony formation assays.

Results: It was determined that increased IRS4 expression led to enhanced radiosensivity in GBM cells. Increased IRS4 expression in the GBM cell line was found to cause a decrease in cell survival rates and colony formation rates.

Conclusion: IRS4 has been identified to potentially play an active role in the radiotherapy response of GBM cells.

Keywords: IRS4, GBM, Radiotherapy

INTRODUCTION

Glioblastoma Multiforme (GBM) is the most common and aggressive brain tumor found in adults.[1] According to the classification by the World Health Organization (WHO), GBM is considered a grade IV tumor with astrocytic differentiation. Its initial symptoms can include various mental changes such as headaches, memory loss, unexplained personality changes, and difficulty in forming sentences.[2] One of the main reasons GBM is among the most lethal cancers is the high level of heterogeneity at the cellular and genetic levels, which limits treatment options.[3] In this context, the average survival time for patients diagnosed with GBM is two years or less.[4] The standard treatment protocol involves the surgical removal of the tumor, followed by chemotherapy combined with radiotherapy (RT), which is considered reasonably safe.[5]

The underlying mechanism of many anti-cancer treatments, including RT or ionizing radiation (IR), is the induction of DNA double-strand breaks (DSBs), which lead to cell death.[6] RT-induced DNA damage causes cell death by inducing multiple death mechanisms, such as apoptosis, necrosis, and senescence.[7] The dose of radiotherapy administered to cancer cells is determined by the genomic structure of the cancer cell and the sensitivity of the surrounding microenvironment to RT.[8]

Insulin has important functions in the central nervous system, and impaired insulin response plays a critical role in the development of neurodegenerative diseases. The insulin receptor (IR), a member of the receptor tyrosine kinase (RTK) family, and the insulin-like growth factor receptor (IGF-IR) are widely expressed in various types of cancer and are generally associated with poor prognosis.[9] Insulin receptor substrate (IRS) proteins are adaptor molecules that regulate multiple cellular processes by transmitting extracellular signals to the intracellular space through transmembrane receptors. intracellular signaling in response to insulin and IGF1 stimulation.[10]

Among the members of the IRS protein family, the expression of IRS4 in tissues is more limited compared to IRS1 and IRS2. Increased IRS4 expression has been associated with various types of cancer, such as breast, lung, colorectal, and hepatocellular cancers. In addition to its expression, genomic studies have shown frequent deletions in the cis-regulatory regions of the IRS4 gene, identifying IRS4 as an oncogenic driver.[11] It has been demonstrated that IRS4, when ectopically expressed via retroviral means, can induce the PI3K signaling pathway even in the absence of growth factors, and despite high levels of IRS1 and IRS2 expression, PI3K has a high affinity for IRS4. This suggests that IRS4 may play a significant role in cancer development.[12]

Numerous studies have provided information on the development of cancer and the response to cancer treatment due to the widespread expression of IRS1 and IRS2, members of the IRS protein family. However, information regarding IRS4 is quite limited. The aim of this study is to explain the fundamental role of the IRS4 protein in the response of GBM cells to radiotherapy.

METHODS

Cell culture
LN229 cell line is p53 mutant, PTEN wild type and p16 and p14ARF deleted was used as the Glioblastoma Multiforme cell model in this study. All cells were cultured as monolayers in DMEM (Dulbecco's Modified Eagle Medium) (Biowest, France) containing 1% L-glutamine (PanBiotech, Germany), 10% Fetal Bovine Serum (Gibco, USA), and 1% PSA (Penicillin-Streptomycin-Amphotericin) (Gibco, USA). The cultures were incubated in a 5% CO_2 atmosphere, 95% humidity, at 37°C.

Radiotherapy treatment
Before radiotherapy treatment, a simulation study was performed for plaque dose planning. The simulation material was covered with tissue-equivalent bolus material with a physical density of 1 g/cm³ and dimensions of 12x8.5x1 cm³ to ensure homogeneous dose distribution in all wells and to represent in-vivo conditions. Axial tomography images with a 2.5 mm slice thickness were obtained from these simulation plaques using the Siemens Sensation 4 model CT-Simulator system. The obtained cross-sectional images were defined in the CMS XIO 3D radiotherapy treatment planning system, and dose planning was conducted using the Theratron 1000E model cobalt-60 teletherapy device. The dose planning was completed for each well using Co-60 photon beams with an average energy of 1.25 MeV, with the cells being exposed to 5, 8, and 10 Gy doses of radiation in a single fraction. The data obtained from the treatment planning system, including field size, SSD (Source Skin Distance), irradiation angles, and irradiation durations, were used for radiotherapy application.

Transfection
LN229 cells were transfected with pcDNA3.1 Flag Tagged human IRS4 or empty pcDNA3.1 plasmids using the Qiagen Attractene Transfection reagent (Qiagen, USA) according to the protocol provided by the manufacturer.

Survival analysis (MTT)
LN229 cells, with increased human IRS4 expression or transfected with control plasmids, were seeded at 5000 cells/well in 96-well plates, with six replicates per condition. After overnight incubation, the cells were treated with 5, 8, and 10 Gray doses of radiotherapy. Following radiotherapy, the cells were incubated for 24, 48, and 72 hours under cell culture conditions. At the end of each incubation period, MTT (Sigma, USA) solution at a concentration of 5 mg/ml was added to each well, and the plates were incubated again for 4 hours under a 5% CO_2 atmosphere at 37°C with 95% humidity. After incubation, the medium was removed, and the resulting formazan crystals were dissolved in 100 µl DMSO. The amount of MTT formazan product was determined by measuring absorbance at 540 nm, with 690 nm as the reference wavelength.

Western blot
Protein lysates from LN229 cells transfected with control and pcDNA3.1 Flag Tagged human IRS4 plasmids were prepared using Triton X-100 buffer containing 50 mM HEPES pH 7.0, 150 mM NaCl, 10% glycerol, 1.2% Triton X-100, 1.5 mM $MgCl_2$, 1 mM EGTA, 10 mM sodium pyrophosphate, 100 mM NaF, 1 mM sodium orthovanadate, 1 mM PMSF, 0.15 units/ml aprotinin, 10 µg/ml leupeptin, and 10 µg/ml pepstatin A. Protein concentrations were determined using the Bradford method, and 100 µg of protein lysates were fractionated by SDS-PAGE and transferred to a PVDF membrane. The membranes were blocked in 5% non-fat dry milk in 1X PBS-Tween 20. Membranes were probed with primary antibodies against IRS4 (Santa-Cruz,USA) and gamma H2AX at a concentration of 1:1000, and Beta-actin (Santa-Cruz,USA) at 1:1500 as a loading control. HRP-conjugated secondary antibodies were used at a concentration of 1:2000, and protein bands were detected using the Image J software. Normalization was performed relative to the beta-actin band.

Colony formation assay

LN229 cells with increased IRS4 expression or transfected with control plasmids were seeded at 500,000 cells/well in 6-well plates. After overnight incubation, one of the plates was treated with 10 Gray radiotherapy, while the other plate was not treated and used as a control. Following radiotherapy treatment, the cells were incubated under cell culture conditions for 9 days, fixed with a methanol acid solution, and stained with a methanol violet solution at a concentration of 0.01% (w/v) for 15 minutes. Colonies were counted using the Image J software.

Statistical analysis

All data from the cell survival and colony formation assays were presented as mean ± standard deviation based on three independent experiments. Multiple comparison analyses were performed using two-way ANOVA with the GraphPad Prism 9 software, and $p < 0.05$ was considered statistically significant.

RESULTS

Effective radiotherapy dose and incubation time for LN229 cells

To determine the effective radiotherapy dose and incubation time, LN229 cells were treated with 5 and 10 Gy doses of radiotherapy and incubated for 48 and 72 hours. Survival analysis results showed a 10% decrease in survival after 48 hours and a 16% decrease after 72 hours in the 5 Gy-treated group compared to the control group. In the 10 Gy-treated group, survival decreased by 16% after 48 hours and 20% after 72 hours compared to the control group (Figure 1).
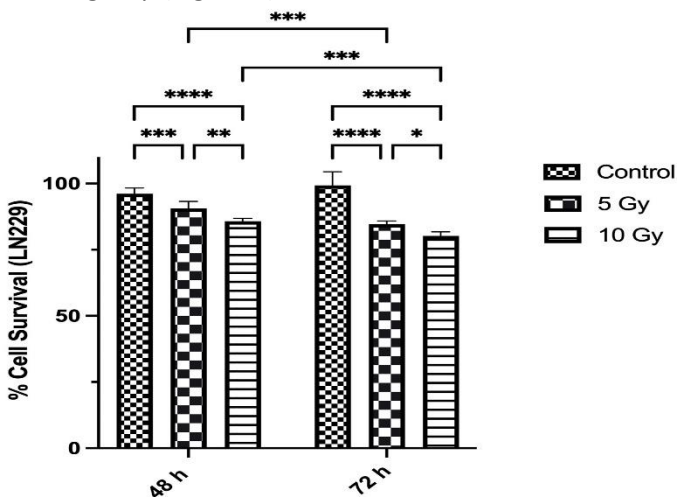
Figure 1. Survival graph of LN229 cells depending on different RT doses and incubation times (*<0.05, **<0.01, ***<0.001, ****<0.0001)

Dose-Dependent γH2AX expression changes in LN229 cells

LN229 cells were treated with 5, 8, and 10 Gy doses of radiotherapy to assess dose-dependent changes in γH2AX expression. A significant increase in γH2AX expression was observed in the 8 and 10 Gy-treated groups compared to the control group, with a 1.5-fold increase in the 10 Gy-treated group correlating with survival analysis results (Figure 2).
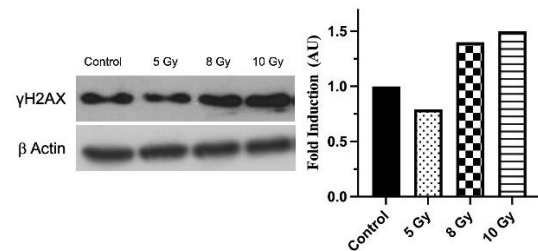
Figure 2. γH2AX expression changes depending on different RT doses in LN229 cells

Effect of IRS4 expression on survival of LN229 cells after radiotherapy

LN229 cells with increased IRS4 expression were treated with a 10 Gy dose of radiotherapy and incubated for 72 hours. No change in survival was observed between the control and pcDNA3.1-transfected groups. However, a 32% decrease in survival was observed in IRS4-expressing LN229 cells without radiotherapy (Figure 3).

In the 10 Gy-treated group, a 25% decrease in survival was observed in IRS4-expressing cells compared to radiotherapy-treated controls, and a 19% decrease compared to non-radiotherapy controls (Figure 3).
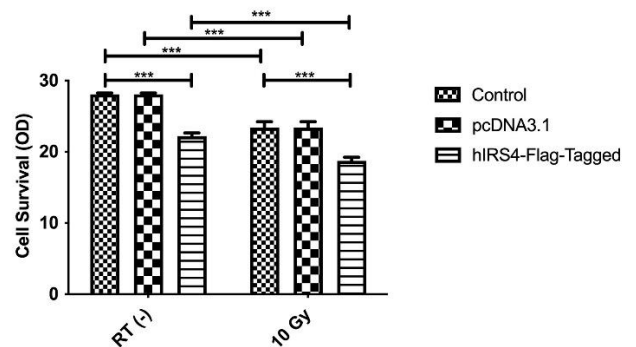
Figure 3. Survival level of IRS4 overexpressing LN229 cells after 10 Gy radiotherapy treatment (***<0.001)

Radiation-Induced γH2AX expression in LN229 cells with increased IRS4 expression

IRS4-transfected LN229 cells were treated with 10 Gy of radiotherapy, and γH2AX expression levels were assessed. A 2-fold increase in phosphorylated γH2AX expression was observed in IRS4-expressing cells compared to control

cells in both radiotherapy-treated groups (Figure 4).
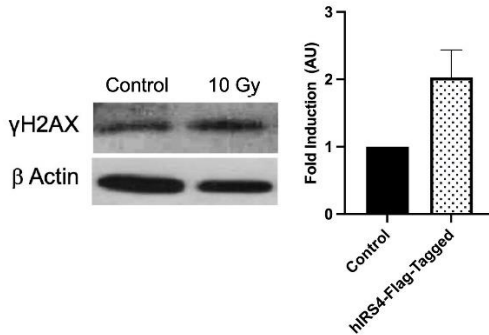
Figure 4. Expression levels of γH2AX after 10 Gy radiotherapy treatment in IRS4 overexpressing LN229 cells

Effect of increased IRS4 expression on colony formation in LN229 cells after radiotherapy

A colony formation assay was performed to compare the colony-forming ability of cells with increased IRS4 expression combined with radiotherapy treatment. A 19% decrease in colony formation was observed in IRS4-expressing LN229 cells compared to controls. In the 10 Gy-treated group, an 88% decrease in colony formation was observed in IRS4-transfected cells compared to controls, and a 98% decrease was observed compared to non-radiotherapy IRS4-expressing cells (Figure 5).
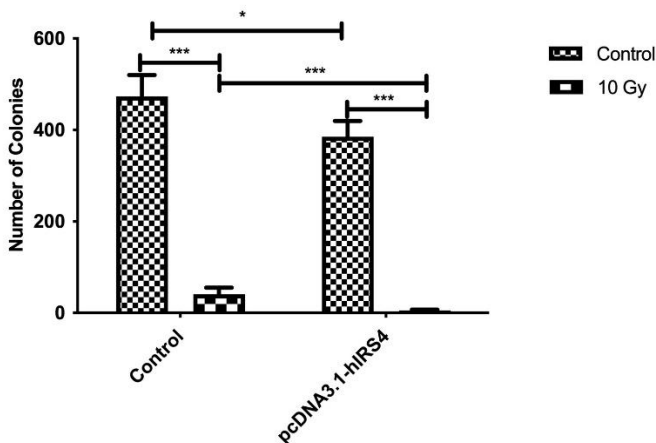
Figure 5. Colony formation rates of IRS4 overexpressing LN229 cells after 10 Gy radiotherapy treatment (*<0.05, ***<0.001)

DISCUSSION

The insulin-like growth factor receptor (IGFR) and insulin receptor (IR) are known to play a role in cancer development and progression. Activation of these signaling pathways by insulin and IGF is common in cancer cells and represents a significant resistance factor to various anticancer therapies.[13]

The tyrosine kinase domains of the IR and IGF-IR β subunits phosphorylate specific substrates such as IRS family members (IRS1-IRS4), Gab-1, Cbl, and Shc. This phosphorylation induces PI3K/AKT/mTOR and ERK/MAPK

pathways, mediating cellular metabolic and mitogenic mechanisms.[14]

Among the IRS family members, IRS4 has limited expression and lacks a protein phosphatase-binding domain, leading to ongoing research into its functional effects.[15] In this study, a 25% decrease in survival was observed in cells treated with a 10 Gy dose of radiotherapy after increased IRS4 expression. The combination of IRS4 transfection and radiotherapy increased the cells' sensitivity to RT. Studies have shown that IRS1 directly binds to Rad51, enhancing DNA repair activity.[16,17] Based on these findings, IRS4, unlike IRS1, may not interact with Rad51, thus not contributing to DNA repair mechanisms. Additionally, studies have shown that IRS4 may inhibit IRS1 function when both proteins are expressed in the same cell.[18] Therefore, increased IRS4 expression in GBM cells may inhibit IRS1 function and reduced DNA repair efficiency.

In subsequent experiments, increased IRS4 expression in cells treated with 10 Gy of radiotherapy was associated with increased γH2AX expression levels compared to controls. This suggests that increased IRS4 expression in cells treated with 10 Gy of radiotherapy may induce cell cycle arrest, senescence, and apoptosis by causing unrepaired DNA damage. γH2AX expression in the control group of IRS4-transfected cells was higher than in the non-transfected control group, suggesting that IRS4 expression may promote DNA damage and cell cycle arrest independent of RT. As a result, increased IRS4 expression alone is sufficient to induce DNA damage and apoptosis in GBM cells, which may be due to reduced IRS1 function and inefficient DNA repair.

This study demonstrated that increased IRS4 expression in GBM cells increases radio sensitivity by reducing DNA repair efficiency. IRS4, which reduces cell survival even without radiotherapy, may be a potential new therapeutic target in GBM treatment. Further experiments using RNA interference methods will contribute to the development of specific treatments targeting IRS4.

REFERENCES

1. Witthayanuwat S, Pesee M, Supaadirek C, Supakalin N, Thamronganantasakul K, Krusun S. Survival analysis of glioblastoma multiforme. *Asian Pac J Cancer Prev.* 2018;19(9):2613–2617. [CrossRef]

2. Dağıstan Y, Dağıstan E, Güney MS. Sebepsiz kişilik değişiklikleri ile başlayan glioblastome multiforme: Bir olgu sunumu. *Abant Tıp Derg.* 2012;1(1):23-25. [CrossRef]

3. Qazi MA, Vora P, Venugopal C, et al. Intratumoral heterogeneity: pathways to treatment resistance and relapse in human glioblastoma. *Ann Oncol.* 2017;28(7):1448-1456. [CrossRef]

4. Burri SH, Gondi V, Brown PD, Mehta MP. The Evolving Role of Tumor Treating Fields in Managing Glioblastoma: Guide for Oncologists. *Am J Clin Oncol.* 2018;41(2):191-196. [CrossRef]

5. Delgado-Martin B, Medina MA. Advances in the Knowledge of the Molecular Biology of Glioblastoma and Its Impact in Patient Diagnosis, Stratification, and Treatment. *Adv Sci (Weinh).* 2020;7(9):1902971. [CrossRef]

6. Pastwa E, Neumann RD, Mezhevaya K, Winters TA. Repair of radiation-induced DNA double-strand breaks is dependent upon radiation quality and the structural complexity of double-strand breaks. *Radiat Res.* 2003;159(2):251-261. [CrossRef]

7. Qiu GH. Protection of the genome and central protein-coding sequences by non-coding DNA against DNA damage from radiation. *Mutat Res Rev Mutat Res.* 2015;764:108-117. [CrossRef]

8. Prasanna PG, Stone HB, Wong RS, et al. Normal tissue protection for improving radiotherapy: Where are the Gaps? *Transl Cancer Res.* 2012;1(1):35-48.

9. Gong Y, Ma Y, Sinyuk M, Loganathan S, et al. Insulin-mediated signaling promotes proliferation and survival of glioblastoma through Akt activation. *Neuro Oncol.* 2016,18(1):48-57. [CrossRef]

10. Machado-Neto JA, Traina F. IRS1 (insulin receptor substrate 1). *Atlas Genet Cytogenet Oncol Hematol.* 2013;17(9):594-598.

11. Sanmartín-Salinas P, Toledo-Lobo MV, Noguerales-Fraguas F, et al. Overexpression of insulin receptor substrate-4 is correlated with clinical staging in colorectal cancer patients. *J Mol Histol.* 2018;49(1):39-49. [CrossRef]

12. Hoxhaj G, Dissanayake K, MacKintosh C. Effect of IRS4 levels on PI3-kinase signalling. *PLoS One.* 2013;8(9):e73327. [CrossRef]

13. Malaguarnera R, Belfiore AThe insulin receptor: a new target for cancer therapy. *Front Endocrinol (Lausanne).* 2011;2:93. [CrossRef]

14. Mendoza MC, Er EE, Blenis J. The Ras-ERK and PI3K-mTOR pathways: cross-talk and compensation. Trends *Biochem Sci.* 2011;36(6):320-328. [CrossRef]

15. Sesti G, Federici M, Hribal ML, Lauro D, Sbraccia P, Lauro R. Defects of the insulin receptor substrate (IRS) system in human metabolic disorders. *FASEB J.* 2001;15(12):2099-111. [CrossRef]

16. Trojanek J, Ho T, Del Valle L, et al. Role of the insulin-like growth factor I/insulin receptor substrate 1 axis in Rad51 trafficking and DNA repair by homologous recombination. *Mol Cell Biol.* 2003,23(21):7510-7524. [CrossRef]

17. Trojanek J, Croul S, Ho T, et al. T-antigen of the human polyomavirus JC attenuates faithful DNA repair by forcing nuclear interaction between IRS-1 and Rad51. *J Cell Physiol.* 2006;06(1):35-46. [CrossRef]

18. Dörpholz G, Murgai A, Jatzlau J, et al. IRS4, a novel modulator of BMP/Smad and Akt signalling during early muscle differentiation. *Sci Rep.* 2017;7(1):8778. [CrossRef]

Circulating Periostin Levels in Osteoporosis and Related Fractures

Halil İbrahim AKBAY[1] iD
Hamit Hakan ALP[1] iD

[1] Department of Biochemistry, Faculty of Medicine, University of Van Yüzüncü Yıl, Van, Türkiye

ABSTRACT

Objective: Periostin, a protein involved in bone remodeling, is linked to osteoporosis. Elevated levels of periostin are associated with an increased risk of fractures due to its role in bone repair and turnover. This meta-analysis aims to investigate the usability of serum periostin levels as a potential biomarker in individuals with osteoporosis and patients at risk of osteoporotic fractures.

Methods: This study was conducted in accordance with the PRISMA guideline. We identified studies reporting periostin levels associated with osteoporosis and osteoporotic fractures through a systematic search in PubMed, Cochrane Library, Web of Science, and Scopus databases. From a total of 175 studies, nine studies meeting the inclusion criteria were included for quantitative synthesis (meta-analysis). Meta-analysis was performed using Revman 5.4.1 software, and forest plots were generated using standardized mean differences (SMD).

Results: When serum periostin levels (ng/mL) were compared between individuals with osteoporosis and healthy controls, periostin levels were found to be significantly higher in patients with osteoporosis (SMD: 1.29, 95% CI: 0.87-1.71). In addition, in the comparison between individuals with and without osteoporosis, periostin levels were found to be significantly higher in patients with fractures (SMD: 11.23, 95% CI: 5.64-16.82). However, significant heterogeneity was observed across studies (I^2: 99% and 72%).

Conclusions: This meta-analysis supports the use of serum periostin levels as a potential biomarker of osteoporosis and osteoporotic fracture risk. However, heterogeneity across studies suggests that caution should be exercised in interpreting these findings. In order for periostin to be more widely used in clinical practice, standardized measurement protocols should be developed and confirmatory studies should be conducted in different populations. periostin to be more widely used in clinical practice, standardized measurement protocols should be developed and confirmatory studies should be conducted in different populations.

Keywords: Bone Mineral Density, Osteoporotic Fractures, Osteoporosis, Periostin

INTRODUCTION

Osteoporosis is a bone disease that is especially common in post-menopausal women and is characterized by a decrease in bone mineral density (BMD) and deterioration of bone microarchitecture.[1] Osteoporosis remains a significant public health concern due to its association with an elevated risk of fractures and a consequent decline in quality of life. Osteoporosis also affects approximately 200 million women worldwide, with a high incidence of fractures in men and women over the age of 50 (one-third of women and one-fifth of men). Osteoporotic fractures not only seriously affect the quality of life, but also cause significant fracture-related morbidity, mortality, and heavy expenses associated with health care management.[2] Periostin is a matricellular protein primarily expressed in connective tissues that are subjected to mechanical loading, such as bones, tendons, and periodontal ligaments.[3] Structurally, periostin is part of the fasciclin family of proteins and plays a pivotal role in maintaining tissue architecture by binding to integrins on cell surfaces, thereby activating several signaling pathways, including Wnt/β-catenin, NF-κB, and FAK.[4] These pathways are involved in cellular proliferation, differentiation, and tissue repair processes.[5] In bones, periostin is highly expressed in the periosteum, where it regulates bone formation and remodeling by promoting osteoblast differentiation and collagen production.[6] This protein's dynamic expression in response to mechanical stress and injury

underscores its importance in skeletal maintenance and repair. In experimental animal studies, it has been stated that periostin plays an important role in differentiation, mineralization and proliferation in osteoblasts.[7]

In studies examining the relationship between periostin and osteoporosis, it has been suggested that periostin expression is upregulated in response to bone injury and may be involved in compensatory mechanisms aimed at increasing bone formation in osteoporotic conditions.[8] In studies examining serum periostin levels, high serum periostin levels have been reported, especially in postmenopausal women with osteoporosis.[9-14] High periostin levels in patients with osteoporosis may also be associated with age, but one study reported that serum periostin did not change significantly from age 30 to 70 but increased in those aged 16-18 and over 70s.[15] The role of periostin in bone tissue and the changes in serum levels in patients with osteoporosis make it a promising candidate for monitoring bone health in these patients and potentially predicting fracture risk.[16,17]

Studies have been conducted to determine the role of serum periostin levels as a biomarker for osteoporosis. In these studies, the correlation between periostin levels and BMD was examined, and while some studies found a negative correlation,[8,14,18] others did not find any correlation.[19-21] The relationship between periostin and osteoporotic fractures has also been investigated, and it has been shown that periostin plays an important role in the early stages of bone healing.[17] Elevated periostin levels are associated with the recruitment of osteoprogenitor cells and new bone formation; these processes are critical for fracture repair.[8,22,23] Studies have shown that periostin levels are significantly increased after fractures, especially in the hip, and may remain elevated throughout the healing process.[18,20,24]

Research Gap and Contribution: Despite the growing body of research on the role of periostin in bone health, particularly in the context of osteoporosis and fractures, the clinical utility of serum periostin as a biomarker remains uncertain. Previous studies have yielded conflicting results regarding its correlation with bone mineral density (BMD) and its potential to predict fracture risk independently of traditional markers. Moreover, the variability in study designs, population characteristics, and periostin measurement methods has led to substantial heterogeneity, complicating the interpretation of findings. This meta-analysis aims to address these gaps by systematically synthesizing the available evidence on serum periostin levels in osteoporosis and related fractures. By consolidating data from multiple studies, this work provides a more comprehensive understanding of periostin's role in bone metabolism and its potential as a biomarker for osteoporosis and fracture risk. This contribution is significant as it seeks to clarify the inconsistencies in the literature and offers insights that could guide future research and clinical practice, ultimately advancing the field of osteoporosis management.

The aim of this meta-analysis is to systematically review and synthesize the available evidence on serum periostin levels in osteoporosis and osteoporotic fractures. The data obtained from this meta-analysis will shed light on whether periostin can be used as a biomarker in both the diagnosis of osteoporosis and the determination of osteoporotic fracture risk.

METHODS
All steps in this meta-analysis were carried out in accordance with the "PRISMA (Systematic Reviews and Meta-Analyses for Preferred Reporting Items)" guideline.

Eligibility criteria
We included studies that measure circulating periostin levels in individuals with osteoporosis, studies that measure serum periostin levels in individuals with fractures, comparative studies between healthy individuals and those with osteoporosis, studies published in peer-reviewed journals, and articles available in English. To minimize heterogeneity, meta-analysis included only studies conducted on plasma and serum samples. All studies used a cross-sectional design in which cases were diagnosed mostly according to BMD T-score, which represents the number of standard deviations below the mean peak bone density of an adult. Specifically, cases were defined by a T-score less than 2.5 standard deviations below peak BMD at the femoral neck or lumbar spine, in accordance with WHO guidelines.

We excluded studies that did not measure circulating periostin levels, animal studies, case reports and reviews, studies without full text, and articles not available in English.

Literature search strategy
An electronic literature search was conducted on May 20, 2024, utilizing the PubMed, Cochrane Library, Web of Science, and Scopus databases. Additionally, a bibliographic scan of the published articles was performed. The search strategy included the following keywords: ("periostin"[MeSH Terms] OR "periostin"[All Fields]) AND ("bone and bones"[MeSH Terms] OR ("bone"[All Fields] AND "bones"[All Fields]) OR "bone and bones"[All Fields] OR "bone"[All Fields]). The articles identified from the search were imported into the Endnote 21 reference manager program (Clarivate Analytics), where duplicate entries were removed.

Two independent researchers reviewed the titles and abstracts for potential eligibility for inclusion in the meta-analysis.

Data extraction

The following information was extracted from the studies included in the meta-analysis; Authors, Year of publication, Study design (e.g., cross-sectional, cohort), sample size, and population characteristics (age, gender, health status). Additionally, the number of participants in each group (osteoporosis, healthy controls, fracture individuals), Mean age and standard deviation, Gender distribution, BMD for relevant anatomical regions (e.g. lumbar spine, hip), Periostin levels (mean ± standard deviation) were also included in the meta-analysis. obtained from the studies.

Study output

The primary outcome of this meta-analysis is to determine the difference in circulating periostin levels between individuals with osteoporosis and healthy controls and between individuals with fractures and those without fractures. The results will be synthesized to provide a comprehensive understanding of the role of periostin in bone health and fracture risk. In particular, we aimed to:
- Compare serum periostin levels between osteoporotic individuals and healthy controls.
- Compare serum periostin levels between people with and without fractures.

Statistical analysis

The meta-analysis was performed using Revman 5.4.1 software. Standardized mean differences were applied to generate forest plots for continuous data. Statistical significance was determined at a threshold of $P < 0.05$, with 95% confidence intervals (CIs) provided. A random-effects model was utilized, and studies were weighted using the generic inverse variance method (Q statistic: $P < 0.10$, $I2 > 50\%$). For meta-analyses that included more than 10 studies, publication bias was assessed according to the recommendations for testing funnel plot asymmetry outlined in the Cochrane Handbook. To assess the robustness of the findings, a sensitivity analysis was conducted by sequentially excluding each study from the analysis for each oxidation marker.

RESULTS

Study selection and characteristics

A systematic search across four major databases—PubMed, Cochrane Library, Web of Science, and Scopus—yielded a total of 175 records. After eliminating duplicates, 75 unique studies remained for screening. The screening process, which involved evaluating titles and abstracts, resulted in the exclusion of 41 studies that did not meet the inclusion criteria. Subsequently, 59 full-text articles were assessed for eligibility. Among these, a significant number of studies were excluded due to various reasons, such as lack of healthy controls, being experimental animal studies, or failure to report periostin levels.

Ultimately, 9 studies met all the eligibility criteria and were included in the quantitative synthesis (meta-analysis) (Figure 1). Detailed demographic information such as the number of participants (N), age, gender distribution (M/F), and BMD values of the control group and osteoporosis patients included in the meta-analysis were summarized in Table 1. The included studies were predominantly cross-sectional in design and covered diverse populations across different geographical regions. The primary focus was on assessing periostin levels in patients with osteoporosis compared to healthy controls, with particular attention to distinguishing patients with and without fractures. This comprehensive meta-analysis serves to consolidate.
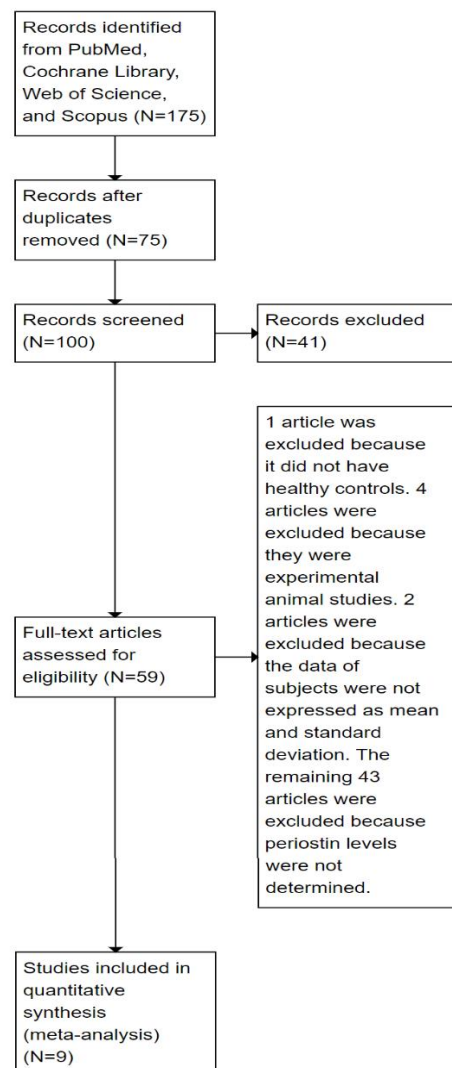

Figure 1. Study Selection Flowchart

Table 1. Overview of Participant Demographics and Bone Mineral Density in Osteoporosis Studies

Studies	Study design	Control group age				Patients with osteoporosis			
		N	Age	Gender M/F	BMD	N	Age	Gender M/F	BMD
Yiğitol et al.[14]	Cross section	30	47.2±10.6	9/21	-	40	50.5 ± 14.0	5/35	-2.15±0.76 (L1-L4 T score)
Li et al. [10]	Cross section	29	55.17±6.59	0/29	0.977±0.085 g/cm^2 (LS)	65	62.17±7.71	0/65	0.726±0.108 g/cm^2 (LS)
Anastasilakis et al.[9]	Prospective cohort	30	65.7 ± 1.4	0/30	-0.75±0.11 (LS)	46	65.7±1.0	0/46	-2.51±0.09
Mahamood et al.[11]	Cross section	25	50.5±6.2	9/16	-0.35±0.4 (LS)	27	52.3±7.1	7/20	-3.48±0.7
Maimoun et al.[12]	Cross section	40	42.6±13.3	17/23	0.925±0.47 g/cm^2 (Total hip)	131	42.8±13.7	8/16	0.690±0.221 g/cm^2 (Total hip)
	Study design	No-Fracture				Fracture			
		N	Age	Gender M/F	BMD	N	Age	Gender M/F	BMD
Bonnet[19]	Cross section	629	65.1±1.5	0/629	0.97±0.18	66	65.0±1.4	0/66	1.07±0.20
Guo[18]	Cross section	315	65.22± 9.71	0/315	0.87 (0.80–0.94)	70	68.10 ± 9.38	0/70	0.78(0.63–0.88)
Pepe[20]	Cross section	25	67.48± 9.51	0/25	0.834 ± 0.167	25	68.64 ± 5.98	0/25	0.818 ± 0.122
Rousseau[24]	Cross section	532	66±8	0/532	0.856±0.12	75	72±9	0/75	0.767±0.11

N: Number of participants, M/F: Number of male/female participants, BMD: Bone mineral density (g/cm²), L1-L4 T score: T scores for the L1-L4 vertebrae, Total hip: BMD value for the hip region, LS: Lumbar spin

Meta-Analysis of periostin levels in osteoporosis

The meta-analysis included data from five studies that compared periostin levels in patients with osteoporosis against healthy controls. The standardized mean difference (SMD) was used as the summary statistic, given the continuous nature of the periostin levels and the need to standardize the effects across studies that may have used different measurement scales.

The pooled mean difference was 1.29 (95% CI: 0.87, 1.71), indicating that periostin levels were significantly higher in osteoporosis patients compared to healthy controls. The data for the comparison are shown as a forest plot in Figure 2. This finding underscores the potential role of periostin as a biomarker for bone metabolism and osteoporosis. Periostin, a matricellular protein involved in bone remodeling, has been implicated in the pathogenesis of osteoporosis due to its role in enhancing osteoblast differentiation and bone formation. The elevated levels observed in osteoporosis patients suggest a compensatory response to bone loss, potentially reflecting an attempt by the body to promote bone repair and remodeling.

Despite the statistically significant findings, there was substantial heterogeneity among the included studies, with

an I² value of 99% and a Q statistic p-value of <0.00001. This high degree of heterogeneity indicates that the effect sizes varied considerably between studies. Several factors may contribute to this variability, including differences in study populations, measurement techniques, and the specific subtypes of osteoporosis assessed. Further subgroup analyses and meta-regression could help elucidate the sources of heterogeneity, although such analyses were beyond the scope of this study due to the limited number of studies included.

Periostin levels in osteoporosis with and without fracture

A separate meta-analysis was conducted to compare periostin levels in osteoporosis patients with fractures versus those without fractures. This analysis included four studies (Figure 3) and revealed a pooled mean difference of 11.23 (95% CI: 5.64, 16.82), indicating significantly higher periostin levels in patients with fractures compared to those without. This finding suggests that periostin may serve as a marker of fracture risk in osteoporosis patients, potentially reflecting increased bone turnover and remodeling activity in response to bone injury.

The heterogeneity in this analysis was moderate, with an I² value of 72% and a Q statistic p-value of 0.01, indicating that while there was some variability in the effect sizes, the

Study or Subgroup	Patients with Osteoporosis			Healthy Control			Weight	Mean difference IV, Fixed, 95% CI	Mean difference IV, Fixed, 95% CI	Risk of Bias A B C D E
	Mean	SD	Total	Mean	SD	Total				
Anastasilakis 2014	272	14	27	250	15	30	0.3%	22.00 [14.47 , 29.53]		+ + − + ?
Li 2021	31.75	16.47	56	26.5	10.11	29	0.6%	5.25 [-0.42 , 10.92]		? + + + ?
Mahmood 2022	2.03	0.78	13	0.92	0.05	25	98.2%	1.11 [0.69 , 1.53]		− ? + ? ?
Maïmoun 2019	784.9	174.2	121	726.6	166.6	40	0.0%	58.30 [-1.94 , 118.54]		+ + + + +
Yigitdol 2023	59.7	11	40	48.9	6.92	27	1.0%	10.80 [6.51 , 15.09]		+ + ? + ?
Total (95% CI)			257			151	100.0%	1.29 [0.87 , 1.71]		

Heterogeneity: Chi² = 53.91, df = 4 (P < 0.00001); I² = 93%
Test for overall effect: Z = 6.03 (P < 0.00001)
Test for subgroup differences: Not applicable

-100 -50 0 50 100
Favours [experimental] Favours [control]

Risk of bias legend
(A) Study population representative of the target group
(B) The response rate adequate
(C) Missing data is specified
(D) Selective reporting (reporting bias)
(E) Other bias

Figure 2. Forest Plot of Periostin Levels in Osteoporosis Patients versus Healthy Controls

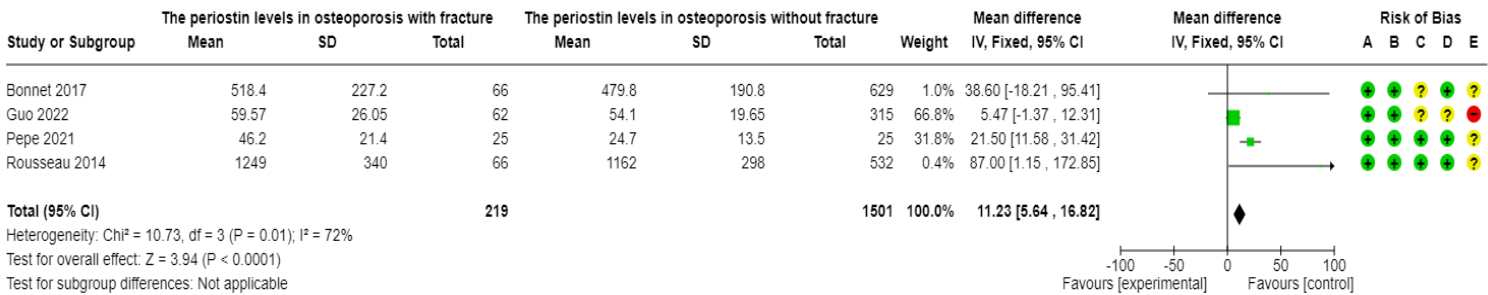| Study or Subgroup	The periostin levels in osteoporosis with fracture			The periostin levels in osteoporosis without fracture			Weight	Mean difference IV, Fixed, 95% CI	Mean difference IV, Fixed, 95% CI	Risk of Bias A B C D E
	Mean	SD	Total	Mean	SD	Total				
Bonnet 2017	518.4	227.2	66	479.8	190.8	629	1.0%	38.60 [-18.21 , 95.41]		+ + ? + ?
Guo 2022	59.57	26.05	62	54.1	19.65	315	66.8%	5.47 [-1.37 , 12.31]		+ + ? ? −
Pepe 2021	46.2	21.4	25	24.7	13.5	25	31.8%	21.50 [11.58 , 31.42]		+ + + + ?
Rousseau 2014	1249	340	66	1162	298	532	0.4%	87.00 [1.15 , 172.85]		+ + + + ?
Total (95% CI)			219			1501	100.0%	11.23 [5.64 , 16.82]		

Heterogeneity: Chi² = 10.73, df = 3 (P = 0.01); I² = 72%
Test for overall effect: Z = 3.94 (P < 0.0001)
Test for subgroup differences: Not applicable

-100 -50 0 50 100
Favours [experimental] Favours [control]

Risk of bias legend
(A) Study population representative of the target group
(B) The response rate adequate
(C) Missing data is specified
(D) Selective reporting (reporting bias)
(E) Other bias

Figure 3. Forest Plot of Periostin Levels in Osteoporosis Patients with Fracture versus Without Fracture

overall trend was consistent across studies. The moderate heterogeneity could be attributed to differences in fracture types, study populations, and periostin measurement techniques.

Publication bias

Publication bias was assessed through funnel plots. The funnel plot for studies comparing periostin levels between osteoporosis patients and healthy controls (Figure 4) appeared relatively symmetrical, suggesting minimal publication bias. However, the interpretation of funnel plots should be approached with caution due to the limited number of studies included.

In contrast, the funnel plot for studies comparing periostin levels between osteoporosis patients with and without fractures (Figure 5) showed slight asymmetry, indicating the possibility of publication bias or small-study effects. This finding, however, must be interpreted cautiously due to the small sample size and potential variability in the included

studies. Further research with larger sample sizes is needed to confirm these findings and assess the robustness of the results.
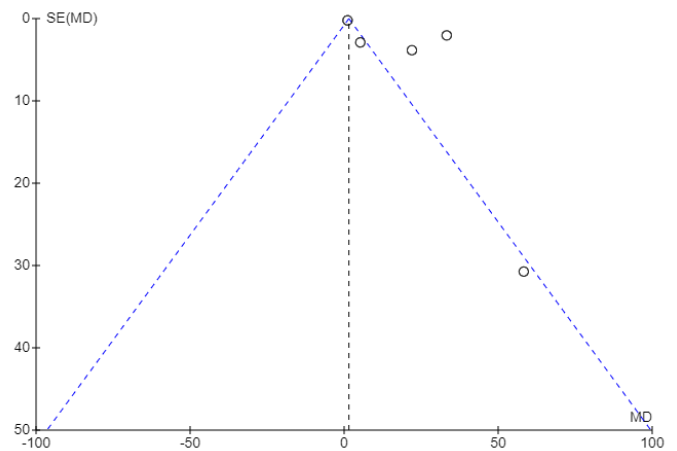
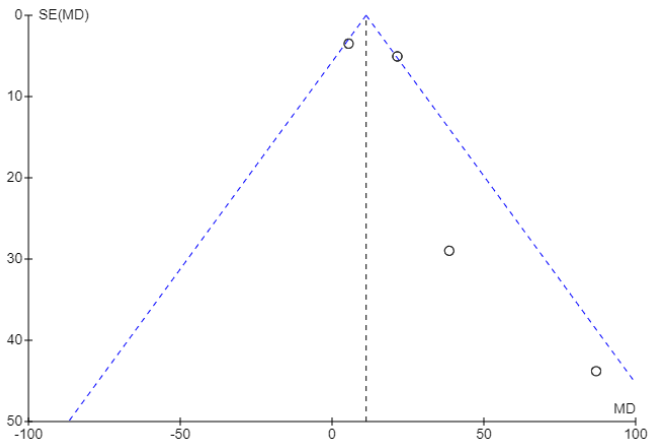**Figure 4.** Funnel Plot for Assessing Publication Bias in Osteoporosis

Figure 5. Funnel Plot for Assessing Publication Bias in Fracture studies

Risk of bias

The risk of bias assessment, conducted according to the Cochrane Handbook guidelines, revealed varying levels of bias across the included studies (Figures 6 and 7). Several studies demonstrated a low risk of bias in key domains, such as the representativeness of the study population and the adequacy of the response rate. However, selective reporting bias emerged as a concern in some studies, with potential implications for the validity of the results. In particular, the selective reporting of outcomes and the failure to pre-specify primary outcomes in some studies could introduce bias and affect the interpretation of the findings.

The summary graph (Figure 6) highlights the distribution of bias across different domains. While the majority of studies had a low risk of bias in terms of the study population and response rate, other areas, such as selective reporting and other potential biases, were more variable. This variability underscores the importance of critically appraising the quality of evidence and considering the risk of bias when interpreting the results of meta-analyses.

Figure 6. Risk of Bias Assessment Across Studies for All Outcomes

Sensitivity analysis

To evaluate the robustness of the findings, a one-study removed sensitivity analysis was conducted. This analysis involved systematically excluding each study from the meta-analysis to assess the impact on the overall effect estimates. The results confirmed that the pooled effect sizes remained consistent, indicating that the findings were robust and not unduly influenced by any single study. This sensitivity

analysis provides additional confidence in the validity of the results and supports the conclusion that periostin levels are significantly associated with osteoporosis and fracture risk.
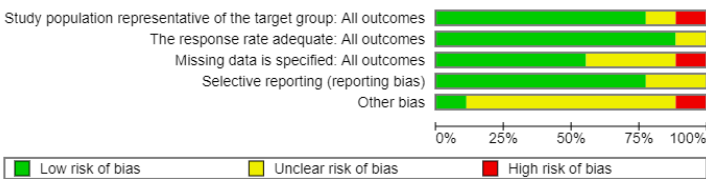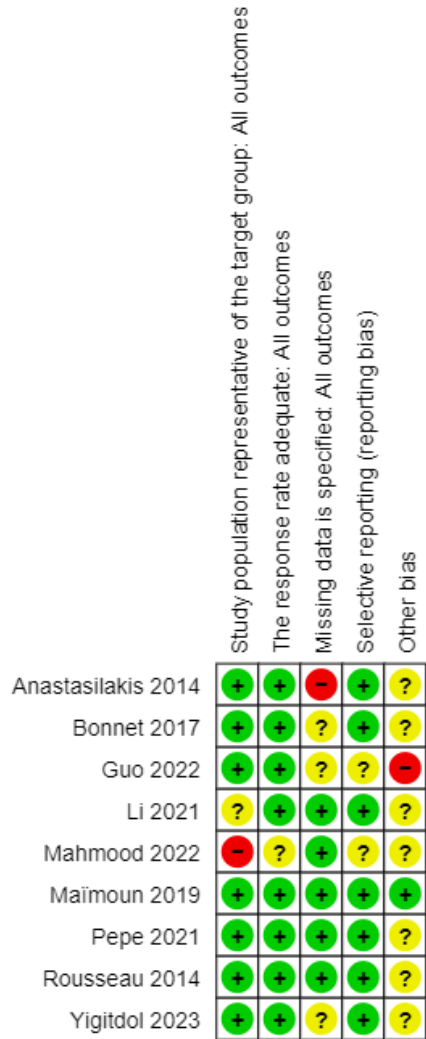

Figure 7. Risk of Bias Summary

DISCUSSION

To our knowledge, this is the first meta-analysis to elucidate and quantify the association of serum periostin levels with fractures in osteoporosis and osteoporosis.

The relationship between bone tissue and periostin has gained the interest of researchers in this field, and studies have been conducted to investigate the function of periostin in bone tissue. Periostin, a matricellular protein encoded by the POSTN gene, plays a critical role in bone metabolism by influencing osteoblast differentiation, migration, and survival. It is primarily expressed in osteocytes and periosteal osteoblasts, contributing to the biomechanical properties of bone through the regulation of collagen cross-linking and fibrillogenic, which is essential for bone strength and

mineralization.[25,26] Additionally, periostin plays a role in the signaling pathways that regulate bone turnover and remodeling. It is also associated with osteogenic differentiation in bone marrow stromal cells, particularly under the influence of estrogen, which is significant in the context of osteoporosis management.[27]

Important results have been obtained in studies examining the relationship between osteoporosis and periostin. Anastasilakis et al. divided postmenopausal osteoporotic women into two groups, low and normal, according to their BMD and examined serum periostin levels and reported that there was no statistically significant difference. Zoledronic acid is a bisphosphonate drug used to prevent bone loss and treat osteoporosis by inhibiting bone resorption. They also reported that zoledronic acid treatment did not affect serum periostin levels. In the same study, although there was no statistically significant difference between the control and treatment groups in baseline serum periostin levels, the periostin levels of the patient treatment group were higher than the control group.[9] Li et al compared periostin levels in patients with type 2 diabetes with normal BMD and those with osteoporosis. As a result, they reported that periostin levels in patients with type 2 diabetes and those with osteoporosis were statistically significantly higher than the periostin levels in patients with type 2 diabetes and normal BMD.[10] In the study conducted by Mahmood and Abbas, they determined the periostin levels in serum samples obtained from the healthy control group (n=25), the osteopenic patient group (n=26) and the osteoporotic patient group (n=27) and reported that the highest periostin levels were observed in the osteoporotic patients and the lowest levels were observed in the healthy control group.[11] Similar to other studies, Maïmoun et al reported that periostin levels were higher in patients with osteoporosis and spinal cord injury than in the control group without spinal cord injury.[12] Mohamed et al compared the periostin levels of Egyptian postmenopausal osteoporotic women with a healthy control group and reported that the periostin levels in the patient group were statistically significantly higher.[13] In their study on patients with primary hyperparathyroidism, Yiğitdol et al reported that the pericytin levels of patients with osteoporosis (n=14) were statistically significantly higher than those without osteoporosis.[14] Li et al compared periostin levels in postmenopausal women with osteoporosis with those in women with normal BMD in the Shanghai, China population and found no statistically significant difference.[21] Yan et al. compared the periostin levels of women with postmenopausal osteoporosis and hip fractures with the control group and reported that the serum periostin levels of patients with hip fractures were statistically significantly higher.[8] In the same study, serum

periostin levels were measured in the period after the fracture and it was reported that periostin levels on the 7th day increased. Since serum periostin levels were given as median in this study, they could not be included in the meta-analysis, and in addition, the deficiencies of the statistical method used in this study were stated by Farrokhi et al.[28]

In summary, the majority of studies investigating periostin levels in individuals with osteoporosis and healthy controls reported that periostin levels were increased in the patient group. The results of this meta-analysis confirm that periostin levels are significantly elevated in individuals with osteoporosis compared to healthy controls. This result supports that periostin may serve as a potential biomarker for osteoporosis and may be useful in the clinical assessment and management of this condition. However, the heterogeneity observed in the studies cannot be ignored and must be taken into consideration when interpreting the results.

The role of serum periostin levels as a biomarker for fracture risk in individuals with osteoporotic fractures has been explored in several studies. The majority of these studies have indicated that periostin has the potential to predict fracture risk independently of bone mineral density (BMD). Rousseau et al. conducted a 7-year prospective study within the OFELY cohort and found that higher serum periostin levels were significantly associated with an increased risk of incident fractures in postmenopausal women, independent of BMD. The study demonstrated that women with periostin levels in the highest quartile had a nearly twofold increased risk of fractures compared to those in lower quartiles. Importantly, the combination of high periostin levels and low hip BMD (T-score ≤ -2.5) markedly increased fracture risk, underscoring the additive value of periostin in fracture risk assessment.[24]

Bonnet et al. expanded on these findings by identifying that a cathepsin K-generated periostin fragment, termed K-periostin, was predictive of incident low-trauma fractures in postmenopausal women, independent of traditional risk factors including BMD and FRAX scores. This study emphasized the role of periostin in bone quality rather than quantity, suggesting that it may reflect microarchitectural deterioration that is not captured by conventional BMD measurements.[19]

Pepe et al. further explored the association between k-periostin levels and fracture risk in postmenopausal women with primary hyperparathyroidism (PHPT). Their findings revealed that women with fractures had significantly higher k-periostin levels compared to those without fractures,

indicating that periostin fragments could serve as an independent marker of bone fragility in this population. This study supports the notion that periostin levels are elevated in conditions of increased bone turnover and remodeling, which are characteristic of PHPT and may contribute to skeletal fragility.[20]

Guo et al. investigated genetic polymorphisms related to periostin and their association with serum periostin levels and fracture risk. They identified specific genetic variants that modulate periostin expression, linking them to an increased predisposition to fractures in individuals with osteoporosis. This genetic perspective adds a layer of complexity to the understanding of periostin's role in bone metabolism and fracture susceptibility.[18] In addition to these studies, a previous study by Xiao et al also stated that the periostin gene may be a candidate in fracture risk assessment.[23]

There are also studies that claim the opposite of the above studies. One of these studies is conducted by Luo and Deng, they stated that there was no significant correlation between serum periostin levels and initial BMD, PTH, P1NP, β-CTx and N-MID-OT levels. Based on their results, they stated that serum periostin levels cannot be used as a biomarker in the initial stage of bone loss in postmenopausal women.[29] In contrast to the findings of elevated periostin levels associated with higher fracture risk, a study by Kerschan-Schindl et al. observed a different pattern in patients with hip fractures undergoing hemi-arthroplasty. This study noted that while periostin levels did increase postoperatively, this increase was primarily interpreted as a marker of bone healing rather than an indicator of fracture risk. The rise in periostin was linked to the natural bone remodeling processes following surgical intervention, rather than being a pre-existing risk factor for fractures. The authors also emphasized that during the bone healing phase, traditional markers like periostin might not accurately reflect overall bone metabolism or fracture susceptibility.[30] Our meta-analysis results demonstrated that individuals with osteoporotic fractures had significantly higher serum periostin levels compared to those without fractures. This result supports the hypothesis that elevated periostin levels may be associated with an increased risk of fractures in osteoporotic patients. However, the presence of substantial heterogeneity among the studies suggests that the relationship between periostin levels and fracture risk may vary depending on the study population and other contextual factors.

In conclusion, considering the comprehensive analysis and synthesis of available data, this meta-analysis concluded that elevated serum periostin levels are consistently associated with osteoporosis and may serve as a promising biomarker for determining fracture risk, although significant variability in study results suggests that further research is needed. This research should aim to standardize measurement techniques and solidify the clinical utility of periostin in osteoporosis management and fracture risk assessment by investigating its role in different populations and contexts. Despite these challenges, the findings highlight the potential of periostin as a valuable tool for understanding bone health dynamics, but its application in routine clinical practice will require careful consideration of the observed heterogeneity.

Limitations

Despite the robust findings presented in this meta-analysis, several limitations should be acknowledged. First, the high degree of heterogeneity observed across studies, particularly in terms of study populations, periostin measurement techniques, and definitions of osteoporosis and fractures, may limit the generalizability of the results. This variability underscores the need for standardized protocols in future research. Second, the meta-analysis was restricted to studies published in English, which may introduce language bias and limit the inclusion of potentially relevant data. Third, the cross-sectional design of most included studies precludes the establishment of a causal relationship between elevated periostin levels and fracture risk. Longitudinal studies are necessary to confirm whether periostin is a reliable predictor of future fractures. One of the other limitations of our study is the presence of different age groups in the meta-analyzed articles. Adding studies in closer age groups may yield clearer and comparable results.

REFERENCES

1. Nih Consensus Panel. Development Panel on Osteoporosis Prevention D, Therapy. Osteoporosis prevention, diagnosis, and therapy. *JAMA*. 2001;285(6):785-795.

2. Anam AK, Insogna K. Update on Osteoporosis Screening and Management. *Med Clin North Am*. 2021;105(6):1117-1134. [CrossRef]

3. Zhu R, Zheng Y, Dirks NL, et al. Model-based clinical pharmacology profiling and exposure-response relationships of the efficacy and biomarker of lebrikizumab in patients with moderate-to-severe

asthma. *Pulm Pharmacol Ther*. 2017;46:88-98. [CrossRef]

4. Yuan C, Li J. Research progress of periostin and osteoporosis. *Front Endocrinol (Lausanne).* 2024;15:1356297. [CrossRef]

5. Hakuno D, Kimura N, Yoshioka M, et al. Periostin advances atherosclerotic and rheumatic cardiac valve degeneration by inducing angiogenesis and MMP production in humans and rodents. *J Clin Invest*. 2010;120(7):2292-2306. [CrossRef]

6. Bonnet N, Garnero P, Ferrari S. Periostin action in bone. *Mol Cell Endocrinol*. 2016;432:75-82. [CrossRef]

7. Yan J, Wang Z, Xian L, et al. Periostin Promotes the Proliferation, Differentiation and Mineralization of Osteoblasts from Ovariectomized Rats. *Horm Metab Res*. 2024. [CrossRef]

8. Yan J, Liu HJ, Li H, et al. Circulating periostin levels increase in association with bone density loss and healing progression during the early phase of hip fracture in Chinese older women. *Osteoporos Int*. 2017;28(8):2335-2341. [CrossRef]

9. Anastasilakis AD, Polyzos SA, Makras P, et al. Circulating periostin levels do not differ between postmenopausal women with normal and low bone mass and are not affected by zoledronic acid treatment. *Horm Metab Res*. 2014;46(2):145-149. [CrossRef]

10. Li J, Niu X, Si Q, et al. Plasma periostin as a biomarker of osteoporosis in postmenopausal women with type 2 diabetes. *J Bone Miner Metab*. 2021;39(4):631-638. [CrossRef]

11. Mahmood H, Abass EAA. Association between periostin and bone minerals in osteoporosis and osteopenia Iraqi patients. *Int. J. Health Sci.*, 2022:9633-9644. [CrossRef]

12. Maïmoun L, Ben Bouallègue F, Gelis A, et al. Periostin and sclerostin levels in individuals with spinal cord injury and their relationship with bone mass, bone turnover, fracture and osteoporosis status. *Bone*. 2019;127:612-619. [CrossRef]

13. Mohamed AS, Khalifa AI, Abotaleb AA-M, Eldesoky NA-R. Comparative Study between Periostin and Osteocalcin as Biomarkers for Osteoporosis and Fracture Risk in Egyptian Postmenopausal Women. *Int J Pharm Pharm Sci*. 2020:17-22.

14. Yigitdol I, Gulumsek E, Ozturk HA, et al. Serum Periostin Levels are Significantly Higher in Patients with Primary Hyperparathyroidism and Closely Related to Osteoporosis. *Exp Clin Endocrinol Diabetes*. 2023;131(9):449-455. [CrossRef]

15. Walsh JS, Gossiel F, Scott JR, Paggiosi MA, Eastell R. Effect of age and gender on serum periostin: Relationship to cortical measures, bone turnover and hormones. *Bone*. 2017;99:8-13. [CrossRef]

16. Garnero P. New developments in biological markers of bone metabolism in osteoporosis. Bone. 2014;66:46-55. [CrossRef]

17. Kim BJ, Lee SH, Koh JM. Potential Biomarkers to Improve the Prediction of Osteoporotic Fractures. *Endocrinol Metab (Seoul)*. 2020;35(1):55-63. [CrossRef]

18. Guo YM, Cheng JH, Zhang H, et al. Serum Periostin Level and Genetic Polymorphisms Are Associated with Vertebral Fracture in Chinese Postmenopausal Women. *Genes (Basel).* 2022;13(3). [CrossRef]

19. Bonnet N, Biver E, Chevalley T, Rizzoli R, Garnero P, Ferrari SL. Serum Levels of a Cathepsin-K Generated Periostin Fragment Predict Incident Low-Trauma Fractures in Postmenopausal Women Independently of BMD and FRAX. *J Bone Miner Res*. 2017;32(11):2232-2238. [CrossRef]

20. Pepe J, Bonnet N, Cipriani C, et al. Higher serum levels of a cathepsin K-generated periostin fragment are associated with fractures in postmenopausal women with primary hyperparathyroidism: a pilot study. *Osteoporos Int*. 2021;32(11):2365-2369. [CrossRef]

21. Li R, Zhu X, Zhang M, Zong G, Zhang K. Association of Serum Periostin Level with Classical Bone Turnover Markers and Bone Mineral Density in Shanghai Chinese Postmenopausal Women with Osteoporosis. *Int J Gen Med*. 2021;14:7639-7646. [CrossRef]

22. Garnero P. The Utility of Biomarkers in Osteoporosis Management. *Mol Diagn Ther.* 2017;21(4):401-418. [CrossRef]

23. Xiao SM, Gao Y, Cheung CL, et al. Association of CDX1 binding site of periostin gene with bone mineral density and vertebral fracture risk. *Osteoporos Int.* 2012;23(7):1877-1887. [CrossRef]

24. Rousseau JC, Sornay-Rendu E, Bertholon C, Chapurlat R, Garnero P. Serum periostin is associated with fracture risk in postmenopausal women: a 7-year prospective analysis of the OFELY study. *J Clin Endocrinol Metab*. 2014;99(7):2533-2539. [CrossRef]

25. Pickering ME, Oris C, Chapurlat R. Periostin in Osteoporosis and Cardiovascular Disease. *J Endocr Soc*. 2023;7(7):bvad081. [CrossRef]

26. Kudo A. Periostin in Bone Biology. *Adv Exp Med Biol*. 2019;1132:43-47. [CrossRef]

27. Li C, Li X, Wang X, et al. Periostin Mediates Oestrogen-Induced Osteogenic Differentiation of Bone Marrow Stromal Cells in Ovariectomised Rats. *Biomed Res Int*. 2020;2020:9405909. [CrossRef]

28. Farrokhi M, Arjaki D, Peykanpour F. Circulating periostin levels increase in association with bone density loss and healing progression during the early phase of hip fracture in Chinese older women. *Osteoporos Int*. 2020;31(10):2061. [CrossRef]

29. Luo J, Deng W. Serum Periostin Level is not a Predictor of Early Stage Bone Loss in Chinese Postmenopausal Women. *Clin Lab*. 2019;65(11). [CrossRef]

30. Kerschan-Schindl K, Tiefenböck TM, Föger-Samwald U, et al. Circulating Myostatin Levels Decrease Transiently after Implantation of a Hip Hemi-Arthroplasty. *Gerontology*. 2020;66(4):393-400. [CrossRef]